Separation and Purification Technology 388 (2026) 136740

Contents lists available at ScienceDirect

Separation and Purification Technology

journal homepage: www.elsevier.com/locate/seppur

Pursuing antifouling performance: Hydrophilic PES-Siloxene membranes for enhanced biological applications

Benjamin Stewart Moore [a], Pablo López-Porfiri [a], Dinesh K. Mahalingam [b,e], Elliot Craddock [a], Abdullah Albiladi [a], Carmine D'Agostino [a], John Chew [b,f], Davide Mattia [b,e], Patricia Gorgojo [a,c,d], María Pérez-Page [a,*]

[a] Department of Chemical Engineering, University of Manchester, Engineering Building A, Booth St E, M13 9PL Manchester, UK
[b] Department of Chemical Engineering, University of Bath, Claverton Down, BA2 7AY Bath, UK
[c] Instituto de Nanociencia y Materiales de Aragón (INMA) CSIC-Universidad de Zaragoza, C/ Mariano Esquillor s/n, 50018 Zaragoza, Spain
[d] Departamento de Ingeniería Química y Tecnologías del Medio Ambiente, Universidad de Zaragoza, C/ Pedro Cerbuna 12, 50009 Zaragoza, Spain
[e] Centre for Integrated Materials, Processes & Structures, University of Bath, Claverton Down, BA2 7AY Bath, UK
[f] Centre for Digital, Manufacturing & Design, University of Bath, Claverton Down, BA2 7AY Bath, UK

ARTICLE INFO

Editor name: Dr. Junyong Zhu

Keywords:
Two-dimensional nanomaterial
Siloxene
Functionalised graphene oxide
Mixed matrix membrane
Fouling

ABSTRACT

Membranes are widely used in biomedical applications due to their efficient separations necessary for a variety of applications, ranging from pre-treatments to hemofiltration. These membranes often suffer fouling from high-concentration biological components, such as blood plasma proteins, which limits the separation performance. However, at research level, they are commonly tested using much lower feed concentrations that are not representative of real conditions. Developing and testing a membrane under high feed concentrations, analogous to those used during practical applications, its fouling resistance can be more realistically assessed.

In this work, siloxene, an easy-to-synthesise hydrophilic, two-dimensional nanomaterial, was successfully incorporated as a filler into the polyethersulfone (PES) membrane matrix. At optimised filler loadings of 0.15 wt %, porosity rose to 83 %, zeta potential was enhanced to −35.4 mV and high hydrophilicity was achieved with a water contact angle as low as 27°. Pure water permeance increased from 75 to 147 LMHBar, compared to PES, while rejecting ~99 % bovine serum albumin (BSA). Furthermore, the flux recovery ratio increased from 17 % to 62 %, therefore improving the use of effective membrane area. PES-siloxene membranes showed significant improvement in their capability to cope with concentrated biological feeds analogous to human blood plasma protein concentration: 80 g L^{-1} BSA solution. PES-Siloxene membranes also superseded the performance of commercial PES "protein-resistant" membrane and functionalised-graphene oxide in an equivalent matrix, highlighted in the literature for its protein antifouling properties. Overall, PES-siloxene MMM results in a low-cost, protein-resistant, and biocompatible membrane that maintains high selectivity suitable for biomedical applications.

1. Introduction

The need for efficient biological separations has presented exponential growth in research on synthetic polymeric membranes within biomedical applications, ranging from drug delivery, tissue engineering, and artificial organs to diagnostic devices, haemodialysis, hemofiltration, and more [1,2]. Pure polymeric membranes have excellent bio-separation capability due to their structural flexibility, adaptable composition, and surface chemistry [3,4]. In particular, polyethersulfone (PES) is commonly used to fabricate nanofiltration (NF)

Abbreviations: AGO, APTS-functionalised GO; APTS, 3-aminopropyltriethoxysilane; ATR-FTIR, Attenuated Total reflectance Fourier transform infrared; BSA, Bovine serum albumin; DCC, N, N′-Dicyclohexylcarbodiimide; DMF, Dimethyl formaldehyde; FRR, Flux recovery ratio; GO, Graphene oxide; MMM, Mixed matrix membrane; MW, Molecular weight; MWCO, Molecular weight cut-off; NF, Nanofiltration; NIPS, Non-solvent-induced phase separation; PEG, Polyethylene glycol; PES, Polyethersulfone; PVP, Polyvinylpyrrolidone; PWP, Pure water permeance; SEM, Scanning electron microscopy; UF, Ultrafiltration; XPS, X-ray photoelectron spectroscopy.

* Corresponding author.
E-mail address: maria.perez-page@manchester.ac.uk (M. Pérez-Page).

https://doi.org/10.1016/j.seppur.2026.136740
Received 1 October 2025; Received in revised form 23 December 2025; Accepted 1 January 2026
Available online 2 January 2026

and ultrafiltration (UF) membranes, displaying outstanding thermal, hydrolytic, and chemical stability, good mechanical properties, moderate cost, commercial availability, and relative hydrophilicity, compared to other polymers, like polysulfone [5,6]. Moreover, PES features for its biocompatibility, imperative in biomedical fields [7]. In certain biomedicine processes, such as haemodialysis and hemofiltration, the relative hydrophobicity of the membrane material composition leads to accelerated fouling due to undesired intermolecular attractions with sugars, fats, proteins, biomolecules, cells, and platelets within biological samples [8]. Biological fouling of membranes is an ongoing issue due to the detrimental impact it has on the membrane's performance and lifetime. For instance, naturally, blood plasma proteins bind on the membrane surface due to hydrophobic interactions with the non-polar sections of the polymeric chain, thus blocking membrane pores and thereby affecting the performance [9,10]. Even though PES membranes are considered a hydrophilic option, these membranes are still prone to this fouling effect, limiting their development in most applications in their natural form [11,12]. To overcome this issue, membranes must be tested under robust conditions of whole blood, e.g., plasma protein content of 60–80 g L^{-1} [13], similar to those used in practical applications. To demonstrate their ability to endure high concentrations of biological foulants while maintaining sufficient function.

Two-dimensional (2D) nanomaterials such as graphene and its derivatives, MXenes, and nanoclays are explored in biomedical studies, including protection against infections and diseases, tissue engineering, diagnostics, drug delivery and more [14,15]. Moreover, 2D nanomaterials have been employed to mitigate membrane fouling either by incorporating them as fillers within the membrane matrix or by applying them as a thin selective layer to modify the membrane surface. The surface modification reduces electrostatic interactions with organic foulants by changing the surface morphology, making fouling less likely [16–18]. Notably, graphene oxide (GO) has shown excellent biocompatibility and has been used in haemodialysis membranes. The functionalities present in its structure, such as hydroxyl, epoxy, carboxyl and carbonyl groups [19,20], enhance hydrophilicity, flux, and solute clearance [21], which can lead to better usability in wearable devices [22]. The increased membrane hydrophilicity reduces its affinity with the proteins, mitigating the fouling at the surface and within its porous network [23]. However, while it has been proven that the incorporation of GO has a positive effect on tailoring membrane performance, large GO loading might agglomerate during membrane fabrication, leading to material defects; hence, its loading must be optimised. The presence of the aforementioned functional groups in the GO allows for functionalisation, incorporating additional beneficial molecular structures, ensuring less filler material is required while further improving the hydrophilicity and avoiding agglomeration [24]. For instance, (3-aminopropyl) triethoxysilane (APTS) functionalised graphene oxide (AGO) further improved the performance of membranes beyond pure GO. Adding hydrophilic amine and ethoxy functional groups to the amphiphilic GO structure enhances the nanomaterial's hydrophilicity and surface roughness. AGO has previously been used in a mixed matrix along with polyvinylidene fluoride for UF [25] and subsequently in a PES matrix capable of NF with reduced membrane fouling [26]. Particularly for this application, adding negatively charged hydrophilic material to a membrane matrix would be beneficial to reduce the accumulation of foulants such as proteins. Plasma proteins are amphiphilic, carrying a net negative charge, and are prone to bind to hydrophobic surfaces [27]. Hence, increased hydrophilicity and an enhanced net negative surface charge will improve the anti-biofouling capabilities of the membrane by mimicking the properties of blood vessels [28], allowing them to repel the proteins, which are responsible for worsening membrane performance in the biomedical context [29].

Among the new materials used as filler in mixed matrix, Siloxene, a silicon-based 2D nanosheet, stands out due to its hydrophilicity. More recently, it was incorporated into a PVDF matrix to induce compaction in PVDF chains, resulting in low free volume and a highly ordered microstructure, producing a membrane with NF properties [30], yielding a 530 Da molecular weight cut-off (MWCO). Siloxene may be favoured over other well-known 2D nanomaterials due to its 2D corrugated structure made of six-membered Si rings connected via Si-O-Si (siloxane) bridges terminated with hydroxy and —H functional groups, and its unique structural and chemical properties [31]. With the planar structure, polar functional groups, high surface area, and interlayer spacing, siloxene has made a significant impact across a wide range of applications, including electrodes within supercapacitors [32], batteries [33], and photocatalysis [34]. Moreover, due to its scalable synthesis technique, based on the de-intercalation of $CaSi_2$ with HCl, it would be well-suited for the material industrial scale-up. The polar siloxane and hydroxy functional groups present in the 2D structure can have favourable interactions with hydrogen bond donors and acceptor molecules in biological sample matrices, hence increasing water affinity and potentially increasing water flux whilst simultaneously reducing biofouling. Supported by the known biocompatibility of analogous siloxene structures [35], a novel combination of a mixed matrix membrane (MMM) of PES and siloxene will help to overcome the drawbacks of their use in biomedical applications.

This work aimed to assess the feasibility of PES-siloxene MMMs for biomedical applications, such as hemofiltration or biological testing pretreatments [36–38], to address challenges related to protein fouling or protein interference, respectively, which is an ongoing issue. Herein, MMMs were fabricated using non-solvent-induced phase separation (NIPS), incorporating siloxene nanofillers into a PES matrix. Pore-former, Polyvinylpyrrolidone (PVP), were incorporated into select PES and PES-Siloxene membranes to enhance pore formation and membrane permeance. Water contact angle, zeta potential, porosity, polyethene glycol (PEG) MWCO, surface and cross-section morphology were assessed as part of the membrane characterisation. Membrane performance was evaluated in terms of pure water permeance (*PWP*), bovine serum albumin (BSA) rejection, and flux recovery tests. Reports assessing protein rejection and membrane biofouling using BSA often use concentrations that are 80–800 times lower than what is present in human blood plasma and are incomparable to real-world biomedical applications. Therefore, to closely simulate real conditions, this article uses an analogous solution of BSA (80 g L^{-1}) as a substitute for human blood plasma. An expectation of ~99 % BSA rejection was set for this material to be considered for biomedical separations, to match the rejection capacity of current commercial biomedical PES membrane options. PES-Siloxene membranes were tested against commercial Biomax® PES, as well as fabricated PES and PES-AGO membranes, as baselines. Biomax® correspond to a UF membrane with high flux and low protein binding. Moreover, PES-AGO has been previously evaluated in our research group, leading to outstanding antifouling performance, achieving a Flux Recovery Ratio (*FRR*) of 64 % [26] at a low protein concentration, and was replicated in this study to measure its performance with concentrated protein feeds, ensuring a fair comparison can be made with siloxene and an already established 2D nanofiller. Altogether, the PES-Siloxene MMM developed will provide a low-cost, protein-resistant, and biocompatible membrane that maintains high selectivity and enhances the applicability for biomedical separation devices. These membranes can withstand the fouling of highly concentrated analogous protein environments while outperforming commercial and literature PES-based membranes.

2. Materials and methods

2.1. Materials

The synthesis of siloxene nanosheets required calcium silicide ($CaSi_2$; technical grade, *Sigma-Aldrich*), sodium hydroxide solution (NaOH; 1 M, *Sigma-Aldrich*), hydrochloric acid solution (HCl; 37 %, *Sigma-Aldrich*), and nylon membrane (pore size 0.45 μm, thickness 100 μm, *Cytiva*). Preparation of MMM required polyethersulfone (PES; 72,000 g mol^{-1},

flakes, *BASF*), polyvinylpyrrolidone (PVP; 40,000 g mol^{-1}, *Sigma-Aldrich*), dimethyl formaldehyde (DMF; ≥ 99.8 %, *Sigma-Aldrich*), and nonwoven fibre support NOVTEXX2471 (*Freudenberg Filtration Technologies*). Synthesis of functionalised graphene oxide required 3-aminopropyltriethoxysilane (APTS; ≥ 98 %, *Sigma-Aldrich*) and N, N′-dicyclohexylcarbodiimide (DCC; 99 %, *Sigma-Aldrich*), and graphene oxide (GO; 10 mg mL^{-1}, William Blythe Ltd). Purification of AGO was carried out using ethanol (≥ 99.9 %, *VWR)*, chloroform ($CHCl_3$; ≥ 99.5 %, *Sigma-Aldrich*) and DMF. Biomax® 50 kDa Membranes (*Sigma-Aldrich*) were used as a commercial PES membrane for comparison. Potassium chloride (KCl; ≥ 99.5 %, *Honeywell*) was used for zeta potential measurements. Protein rejection and fouling experiments required BSA (~66,000 g mol^{-1}, *Sigma-Aldrich*). PEG (300, 3,000, 10,000, and 35,000 g mol^{-1}, technical grade, *Sigma-Aldrich*). All materials were used as received. Chemical structures of PES, siloxene, and PVP are depicted in Fig. 1.

2.2. Synthesis and characterisation of 2D filler materials

2D siloxene nanosheets were synthesised in a topochemical deintercalation reaction of $CaSi_2$ and HCl at 0 °C [30]. In a typical reaction, 3 g of $CaSi_2$ powder was pretreated with 1 M NaOH solution at room temperature (24 h) to remove any silicon crystal impurities. The product mixture was washed with DI water under vacuum filtration on a nylon membrane until the pH was neutral. The purified $CaSi_2$ was then dried at 80 °C for 12 h.

The dried $CaSi_2$ powder from the previous reaction step was added to a double-jacketed reaction flask pre-chilled with 300 mL of concentrated HCl solution, stirred vigorously at 0 °C for 4 days (black to yellow-green colour change). The mixture was then diluted and washed with DI water until the pH of the solution was neutral. The crude siloxene product was filtered under vacuum through a 10–15 µm sintered funnel lined with a porous nylon support membrane. Washing with DI water and acetone removed the remaining HCl and $CaCl_2$ impurities. The siloxene was dispersed in 350 mL of ultrapure water before being purified by dialysis (3,500 Da) in a plastic tank with constant gentle stirring for 48 h. DI water was changed every 24 h. The product was diluted to 1 L of ultrapure water before use, and then the appropriate amount was dried when needed. Raman spectra of siloxene powder were collected using a Renishaw inVia confocal Raman microscope, using a 532 nm laser. Surface morphology images of the 2D siloxene nanosheets were collected using scanning electron microscopy (SEM) on a FEI Quanta 250 FEG-SEM with Gatan 3view. Transition electron microscopy (TEM) images were collected using the High Resolution TEM (JEM-2100Plus, JEOL). Attenuated total reflectance-Fourier transform infrared (ATR-FTIR) analysis was conducted using a Bruker Vertex 70 FTIR system-ATR measurements from 4000 to 400 cm^{-1}.

The comparative AGO was synthesised using a method detailed by Luque-Alled et al. [26] and characterised using ATR-FTIR, SEM, and XPS analysis as shown in the Supporting Information (*2. Synthesis and Characterisation of 3-aminopropyltriethoxysilane functionalised Graphene Oxide (AGO)*).

2.3. Membrane fabrication and characterisation

2.3.1. Membrane fabrication

PES membranes were prepared using the non-solvent induced phase separation (NIPS) method, both as neat membranes and with nanofillers at various concentrations, as detailed in Table 1. Homogeneous casting solutions of PES (20 wt%) in DMF were prepared using a shaker plate for at least 12 h to aid solvation. To achieve the evaluated filler percentages (0.025–0.250 wt%), 1 wt% siloxene was dispersed in DMF using a sonication probe. The corresponding amount of siloxene dispersion was added to the PES-DMF solution and stirred magnetically for at least 3 h to ensure uniform distribution before casting. The solutions were cast using a film casting knife with a 150 µm air gap with a sheer rate of 50 mm s^{-1} on an Elcometer 4340 Automatic Film Applicator. Membranes for testing *PWP*, BSA rejection, and antifouling capabilities were cast onto nonwoven fibre support, while it was necessary to cast some freestanding membranes for other characterisation purposes. The fabricated membranes were immediately immersed in a non-solvent coagulation bath containing DI water. After 10 min, the membrane was removed from the non-solvent bath, washed with DI water, and then

Table 1
Composition of casting solutions used to fabricate PES-based MMM.

Membranes	Concentration / wt%				
	PES	Siloxene	AGO	PVP	DMF
PES	20.00	–	–	–	80.000
3PVP	20.00	–	–	3.000	77.000
0.025Si	20.00	0.025	–	–	79.975
0.050Si	20.00	0.050	–	–	79.950
0.100Si	20.00	0.100	–	–	79.900
0.150Si	20.00	0.150	–	–	79.850
0.250Si	20.00	0.250	–	–	79.750
0.150Si_3PVP	20.00	0.150	–	3.00	76.850
0.100AGO	20.00	–	0.10	–	79.900
0.100AGO_3PVP	20.00	–	0.10	3.00	76.900

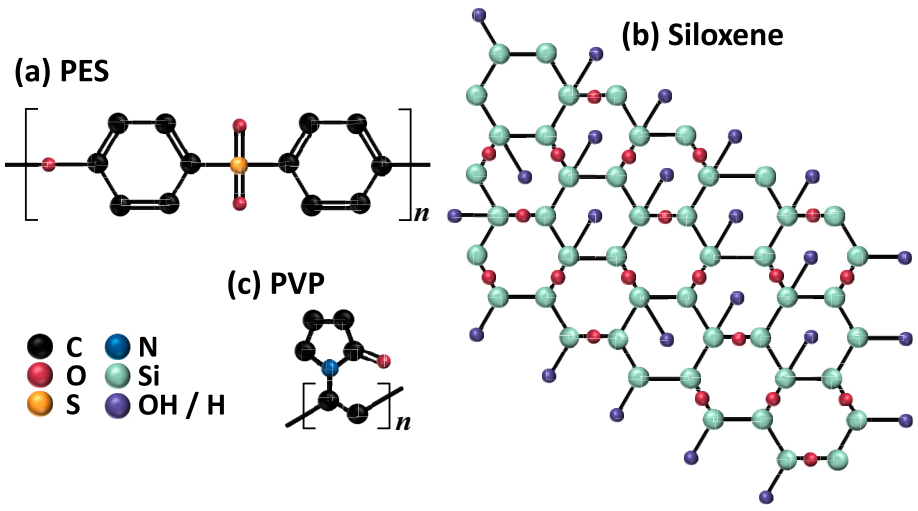

Fig. 1. Illustrations of (a) Polyethersulfone (PES), the base polymer used throughout this study for membrane fabrication; (b) Siloxene, a silicon and oxygen-based 2D nanomaterial, is used as a nanofiller; (c) Polyvinylpyrrolidone (PVP), the pore-forming additive added to PES and PES-Siloxene membrane.

stored in DI water until the membranes were evaluated.

A pore-forming agent, PVP, was added to select PES, PES-Siloxene and PES-AGO membranes before the nanofillers were added, but after their PES-DMF casting solutions were homogeneous. The chosen membrane compositions included the base cases PES and PES-AGO, and the best performing PES-Siloxene membrane, determined by the hydrophilicity, surface charge, *PWP*, and BSA rejection.

A broad range of siloxene loadings was used to identify the favoured concentrations exhibiting the best membrane performance. PVP pore-formers were added to the PES-Siloxene membrane with the most favourable loading to assess any improvements to pore formation and permeance. PES-AGO membranes were fabricated to provide a base case 2D nanomaterial to compare with the PES-Siloxene membranes. PES-AGO were previously proven to possess good protein antifouling properties; however, replication was necessary to evaluate their performance under high protein concentrations [26].

2.3.2. Membrane characterisation

Surface and cross-section morphology of the membranes was analysed using SEM on FEI Quanta 250 FEG-SEM with Gatan 3view. Cross-section images were collected using freestanding (unsupported) membranes that were broken via cryo-fracturing in liquid nitrogen.

Effective membrane thickness was measured using a Mitutoyo IP65 micrometre, taking the average of five points on the membrane casting sheet and subtracting the thickness of the support (170 μm).

The porosity (ε, %) of the membranes was measured using a gravimetric method over an average of three measurements, according to Eq. 1, where W_w is the weight of the wet membrane, W_d is the weight of the dry membrane, ρ_w is the density of water (0.998 g cm^{-3}), and ρ_p is the density of the PES polymer (1.370 g cm^{-3}) [39]. Non-supported membranes were cut into approximately 1 cm^2 squares and hydrated in DI water for at least 1 h. Once removed from the DI water, excess surface water was removed using tissue paper before weighing, to assess the mass of water uptake in the membrane's pores. These membranes were dried in a vacuum oven at 40 °C for 2 h. The membranes were then weighed again.

$$\varepsilon = \frac{\frac{W_w - W_d}{\rho_w}}{\frac{W_w - W_d}{\rho_w} + \frac{W_d}{\rho_p}} \times 100 \left(\% \right) \tag{1}$$

Sessile drop measurements were collected using a Biolin Scientific Theta Lite optical tensiometer using ultrapure Type 1 water to measure the water contact angle. Measurements were made in triplicate.

The surface charge of the membrane was measured as the zeta potential using an Electrokinetic Analyser (Anton Paar Surpass3) equipped with a film-measuring clamping cell. The measurements were carried out using a streaming potential method with a KCl electrolyte solution (0.01 M), with a gap height of 100 μm and a pH of ~7. Zeta potential (mV) was calculated according to the Helmholtz-Smoluchowski equation (Eq. 2):

$$\zeta = \frac{dU}{dp} \times \frac{\eta}{\varepsilon_d \times \varepsilon_{d0}} \times \frac{L}{A} \times \frac{1}{R} \tag{2}$$

where $\frac{dU}{dp}$ is the gradient of the streaming potential (mV) against the differential pressure (600–200, mBar), η is electrolyte viscosity (kg m^{-1} s^{-1}), ε_d is the dielectric coefficient of the electrolyte, ε_{d0} is the permittivity, L is the streaming channel length (m), A is the cross-section of the streaming channel (m), and R is the measuring cell resistance (Ω).

Sponge-like material pore sizes (d_{pore}/m) of the MMMs were measured by capillary flow porometry using an IB-FT Porolux™ 1000 porometer using Porefil® (19.00 mN m^{-1}) as the wetting liquid [40]. The macrovoid-to-sponge-like material ratio was calculated using the cross-sectional areas of the macrovoids and sponge-like material taken from the SEM analysis.

The rejection (R, %) capability of the membranes and the MWCO for the membranes were analysed using PEG molecules with different molecular weights. A mixed solution of PEG (300, 3,000, 10,000 and 35,000 g mol^{-1}) was prepared at 1 g L^{-1} each in deionised water. PEG rejection tests were carried out in a stirred dead-end filtration cell (Sterlitech HP4750) at a transmembrane pressure of 4 bar (± 0.05). Concentrations of both the PEG feed and permeate were determined using Agilent gel permeation chromatography (GPC) with a series of columns, PL aquagel−OH 20 8 μm, and a 300 × 7.5 mm (p/n PL1120–6830). A 20 μL injection volume was used, at a flow rate of 1 mL min^{-1} and temperature of 35 °C, using ultrapure Type 1 water as eluent. Rejection was calculated using Eq. 3, where C_p is the permeate concentration and C_f is the feed concentration, in g L^{-1}. Measurements were made in triplicate, and an average was taken.

$$R = \left(1 - \frac{C_p}{C_f}\right) \times 100(\%) \tag{3}$$

2.3.3. Evaluation of membrane performance

Pure water permeance (*PWP*, L m^{-2} h^{-1} bar^{-1} (LMHBar)) was measured using a stirred dead-end filtration cell (Sterlitech HP4750) connected to a pressurised airline. Tests were carried out at room temperature with an effective area of 1.27 cm^2 and a pressure of 4 (± 0.05) bar. Using DI water, permeation was measured until the values reached a steady state flux equilibrium. *PWP* was then calculated according to Eq. 4, where V is the permeate volume (L), A is the membrane surface area (m^2), t is time (h), and p is pressure (bar).

$$PWP = \frac{\left(\frac{V}{A \times t}\right)}{p} \tag{4}$$

Blood plasma proteins are the main components responsible for fouling in biomedical separations. These proteins are present at concentrations ranging from 60 to 80 g L^{-1}, averaging 72 g L^{-1} in a regular adult, of which human serum albumin (HSA, 35–40 g L^{-1}) is the most abundant of these proteins [13]. HSA is the smallest of the most abundant proteins, yet it is still relatively large with a molecular weight of 69 kDa, making it a solute that can be sufficiently retained using UF membranes, but membrane performance may be diminished due to the formation of a thick cake layer resulting from protein fouling. Bovine serum albumin (BSA) can be used as an appropriate analogue due to its comparable size (66.5 kDa) and properties to human proteins [41]. It is worth noting that HSA is overall more hydrophobic than BSA, meaning that BSA will more readily foul on a hydrophilic surface. Nevertheless, this does suggest that the fouling resistance to HSA of the fabricated membranes would be greater than that of BSA.

Reports on BSA protein rejection and fouling studies commonly use a BSA concentration of just 1 g L^{-1} or lower, which is not representative of assessments typically conducted for genuine biomedical applications. Therefore, this work uses an analogous solution of BSA at 80 g L^{-1} as a model solution for human blood plasma [13]. It was chosen to extrapolate the BSA to match the whole plasma protein concentration rather than just match the HSA concentration. This would give a better approximation of the fouling a membrane may experience during processes like hemofiltration, which requires the retention of the albumin protein.

Separation tests were carried out in a stirred dead-end filtration cell (Sterlitech HP4750) using the same membrane dimensions and conditions as the *PWP* tests, for approximately 2 h. Feed BSA solutions were prepared using ultrapure water. The feed and permeate concentrations of BSA were measured using a UV–Vis spectrophotometer (Jenway 7415) at a wavelength of 280 nm. Calibration curves of the BSA feed solution can be found in Fig. S5. Rejection (R, %) of both BSA and PEG was calculated using Eq. (3).

Membrane antifouling assessments were conducted using a crossflow module to reflect practical application testing. The flow rate of the feed

solution was 3.1 L h^{-1}, with a crossflow velocity of 0.590 m s^{-1}, and a feed volume of up to 2 L. This involves measuring the *PWP* at 4 bar (± 0.05) for 30 min (PWP_1) followed by the permeation of the model BSA solution (80 g L^{-1}) for 30 min at 4 bar (± 0.05) (J_{BSA}). The membrane was then rinsed with DI water, and the PWP was measured again at 4 bar (± 0.05) for 30 min (PWP_2). From these values (PWP_1, J_{BSA}, and PWP_2), the fouling parameters can be calculated. Flux recovery ratio (*FRR*), the % of water permeation that is recovered after BSA permeation and washing; total flux decline ratio (R_t), the % decline of permeation when permeating using a BSA/water feed; reversible flux decline ratio (R_r); and irreversible flux decline ratio (R_{ir}), were calculated using Eq.(5), Eq. (6), Eq.(7), and Eq.(8), respectively:

$$FRR = \left(\frac{PWP_2}{PWP_1}\right) \times 100 \quad (5)$$

$$R_t = \left(1 - \frac{J_{BSA}}{PWP_1}\right) \times 100 \quad (6)$$

$$R_r = \left(\frac{PWP_2 - J_{BSA}}{PWP_1}\right) \times 100 \quad (7)$$

$$R_{ir} = \left(\frac{PWP_1 - PWP_2}{PWP_1}\right) \times 100 \quad (8)$$

A long-term BSA permeance experiment was conducted in a stirred dead-end filtration cell (Sterlitech HP4750) using the same membrane dimensions and conditions as the *PWP* tests, monitoring 4 h of permeation. Tests were carried out using the 80 g L^{-1} BSA model solution. 4 h was chosen to reflect performance in long-term applications such as hemofiltration or haemodialysis, which typically last between 3 and 4 h (according to NHS UK) [42].

3. Results and discussion

3.1. Material characterisation

The successful synthesis of the 2D nanomaterials used in this study was confirmed using Raman spectroscopy, ATR-FTIR, SEM and XPS analysis, as shown in the Supporting Information (Fig. S1 to S4).

3.2. Membrane characterisation

3.2.1. Membrane morphology

The cross-sectional membrane morphology of PES and MMM, in Fig. 2, shows that the fabricated membranes displayed an asymmetrical structure, with a dense top selective layer, followed by a porous sub-layer made up of a sponge-like structure with finger-like macrovoids throughout. Cross-sectional images of base PES membranes display that

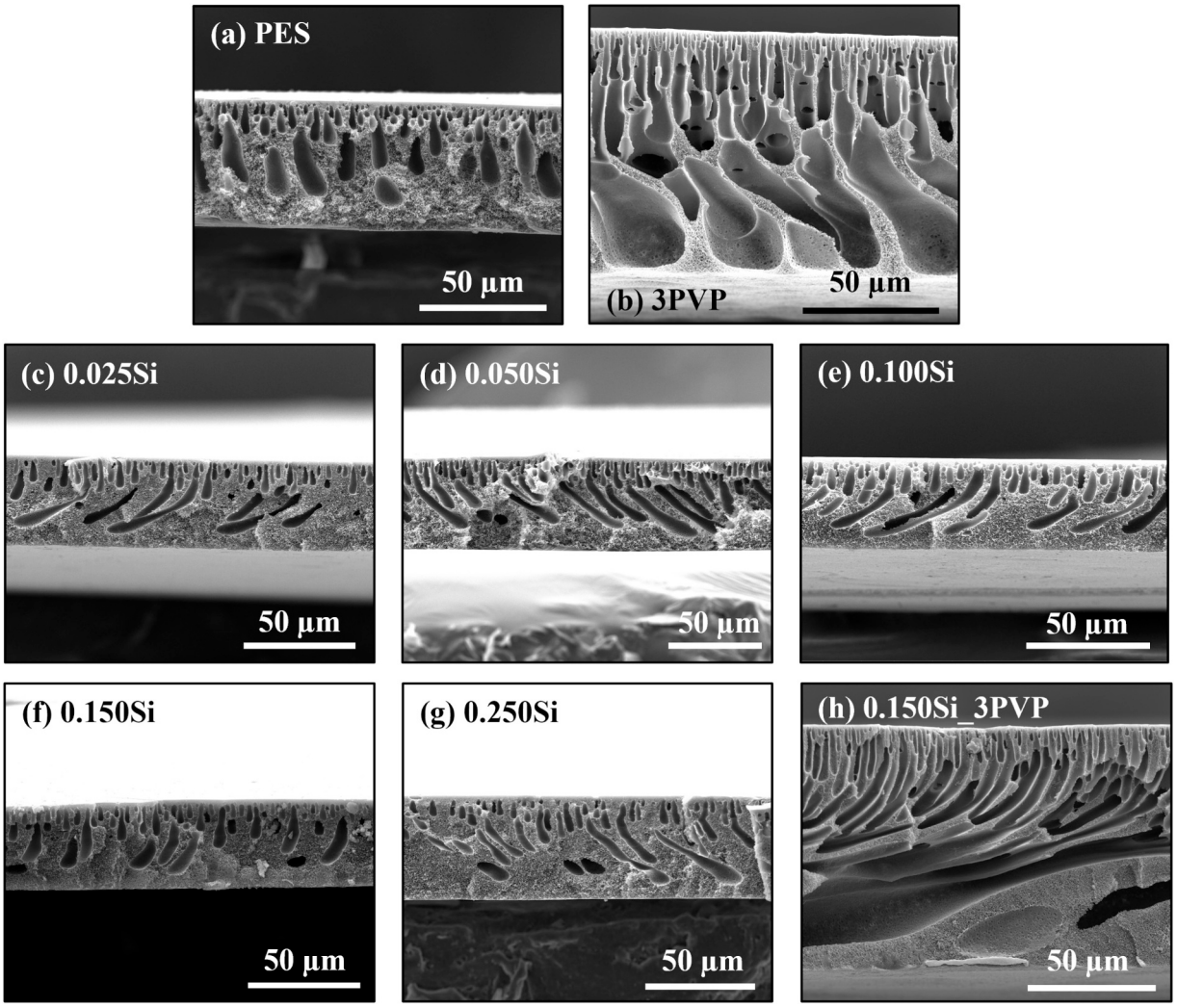

Fig. 2. Cross-section SEM images of PES-based membranes: (a) Base PES, (b) PES with PVP pore-former, (c)-(g) PES-Siloxene at different siloxene concentrations, and (h) PES-Siloxene with PVP pore-former. Each scale bar is equivalent to 50 µm.

the macrovoids are short and do not penetrate completely through the membrane structure (Fig. 2a) [19].

The addition of siloxene loadings to the PES matrix exhibited slight changes in macrovoid structure, characterised by a reduction in void width and an increase in their number and length, extending deeper into the asymmetric membrane structure (Fig. 2c-g). However, there is no obvious difference between the morphologies at different filler concentrations. It would be expected that the reduction in macrovoids would reduce the total mass transfer due to increased resistance from the sponge-like structure and an increase in the virtual total path length of permeating molecules [43]. An increase in the hydrophilicity imparted by the filler can compensate for this, which can reduce the repulsion of other hydrophilic molecules, e.g., water, and aid in surface diffusion through the inner structure walls of the membrane [43,44].

With the addition of 3 wt% PVP, a pore-forming material, a distinct change in the membrane structure was observed (Fig. 2b & 2h). The selective skin layer at the surface is visibly much thinner. While the overall structure consists of much less sponge-like material, substantially more macrovoids and almost doubles in thickness. Visible change in the membrane cross-sectional morphology is induced by the very hydrophilic composition of the PVP polymer, causing the solvent/non-solvent exchange during non-solvent-induced phase separation to occur much faster, which generates thin surface layers and larger macrovoids [45]. The PVP acts as a polymer surfactant, whereby the carbonyl group orients toward the solvent while the alkyl chain orients toward the polymer, compressing the PES in solution and reducing its hydrodynamic volume; creating larger macrovoids that now cover most of the cross-section, and the visibly denser sponge-like composition [46]. A reduction in the skin layer at the surface of the membrane with a substantial increase in the size and number of the macrovoids should reduce the overall mass transfer resistance. Enhancing the permeation throughout the dense polymeric surface and diffusion through the porous substructure [43]. However, this could substantially reduce membrane rejection, a prime example of the permeance and rejection trade-off [47].

Surface morphology of the membranes appeared uniform and remained consistent across all samples, akin to the dense top layer of the cross-section morphology (see Fig. S6d-g). Images of the commercial PES Biomax® membranes are reported as well (see Fig. S7 and Fig. S8). These membranes exhibit a smooth, dense surface layer, but the porous substructure is made up of purely dense sponge-like morphology with no macrovoids. Moreover, the dense skin layer at the cross-section surface appears more porous than that of the membranes fabricated via NIPS.

Membranes containing PVP pore former are approximately double the thickness of the membranes without the pore former, as shown by the thickness measurements in Fig. 3a. Again, the PVP takes a more effective role in the NIPS process. The increased hydrophilicity, compared to PES, ensures more contact with the non-solvent (water) phase during the phase inversion process. This creates larger voids that increase the thickness of the overall structure [48]. In these cases, the filler material has less impact on the resultant cross-sectional morphology. The average thickness of most membranes does show a trend, yet there is no significant change due to the associated error. Nevertheless, the addition of siloxene shows a proportional reduction in the average membrane thickness. The average thickness of 0.150Si dropped to 21.8 (± 3.8) μm from 28.6 (± 4.3) μm in the PES membrane. While there is still a dense skin surface, the reduced thickness of the membrane should offer less resistance to water transport during permeance testing.

The addition of 2D nanosheets to polymer matrices with favourable hydrogen bonding interactions induces a better polymer chain organisation [49,50]. Interactions between the polymer and the 2D nanosheet reduce the interfacial distance between them, promoting a higher polymer chain packing, better compatibility and dispersion within the membrane matrix, resulting in a reduced thickness upon the addition of 2D siloxene nanosheets. However, when the siloxene concentration increased from 0.15 to 0.25 wt%, the thickness increased, potentially suggesting the presence of an optimal concentration and reduced effectiveness of siloxene at concentrations around 0.15 wt%. As filler concentrations increase, there is the risk of agglomeration in the matrix; this is because the highly polar structure of the siloxene forms hydrogen bonds with itself, worsening the dispersion and reducing the effectiveness of the siloxene and ultimately increasing the average thickness [51]. When siloxene was incorporated into PVDF membranes at concentrations of 0.10 wt% and above, agglomerates were observed on the membrane surface, as previously reported in the literature [30,52]. Evidence of siloxene agglomeration in 0.250Si can be observed in Fig. S6a-c, where an agglomerated piece of the material is visible inside a macrovoid in the substructure. Agglomerated flakes of siloxene were not visible in any of the other membrane cross-sectional images due to

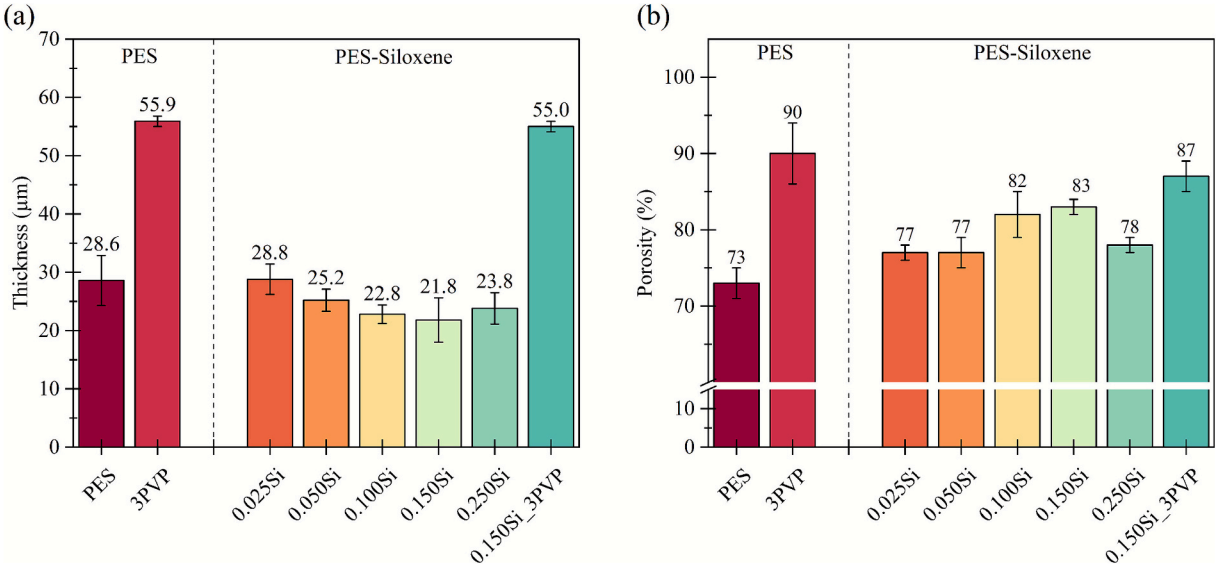

Fig. 3. (a) Thickness of PES and PES-filler MMMs selective layer studied in this work. The selective layer thickness was obtained by subtracting the thickness of the nonwoven support from the thickness of the cast membrane, measured in five different points; **(b)** Porosity (%) of PES and derivative MMMs. A portion of the water-saturated membrane was weighed before being completely dried and then weighed again. Inputting the values into Eq. 1, along with the density of PES, resulted in the porosity.

the good dispersion and relatively low content within the membrane.

It is evident from the data displayed in Fig. 3b that the addition of small amounts of hydrophilic 2D filler materials to the PES matrix increases the porosity. The enhanced hydrogen bonding due to the presence of siloxene throughout the casting solution speeds up the rate of inward water diffusion during casting and, therefore, the rate of outward solvent diffusion, creating larger and more frequent macrovoids that are responsible for increasing porosity [53]. The base PES membrane had a porosity of 73 % (± 2 %), rising to 83 % (± 1 %) (0.150Si) with increasing addition of siloxene before declining due to siloxene agglomeration, reducing its effectiveness. For those membranes with the PVP additive, the porosity was higher than their additive-free counterparts, due to the substantial hydrophilicity of the PVP molecule, inducing even faster phase separation [48]. 3PVP had a porosity reaching 90 % (± 4 %), whilst 0.150Si_3PVP saw a small comparative reduction. Favourable interactions between hydrophilic groups of the PVP and the siloxene would slow phase separation, which explains this modest change [26]. The increased membrane porosity will facilitate mass transfer through the internal structure due to larger macrovoids. This offers reduced resistance compared to the sponge-like morphology, thereby leading to increased permeance.

Moreover, the sponge-like material size analysis and Macrovoids/Sponge-like material ratios in Table 2 gave some insight into the changes seen in the MMMs. As evident by the sponge-like material size analysis, there is some statistically significant change between the base PES, PES-PVP, PES-Siloxene, and PES-Siloxene-PVP. The actual change seems to be minimal, suggesting both materials had little impact on the pore size. However, the bigger changes can be seen in the Macrovoids/Sponge-like material ratio, with the PVP-containing membranes having a substantial increase in the macrovoids, further confirming the changes seen in the SEM images. The PES-Siloxene membranes saw minimal change in this analysis, having a similar Macrovoids/Sponge-like material ratio to the base PES. Moreover, the SEM images show a change to the shape of the macrovoids, rather than a change to their size or number. A complete summary of the raw data collected from the Porolux™ 1000 can be found in Table S1 and Table S2 in the Supporting Information.

MWCO can be an effective method to show the rejection capacity and information on the pore size of a membrane, where an UF membrane is expected to have a MWCO of anywhere between 10 and 100 kDa [54] and an NF membrane between 500 and 200 Da [55]. The PEG rejection results in Fig. 4 suggest that the PES-Siloxene membranes have a UF performance, which can be further supported by the BSA rejection. Altogether, the results suggest a cut-off between 35,000 and 65,500 g mol^{-1}, as the BSA shows almost complete rejection. BSA rejections are presented fully in a later section, *3.3.1 Pure Water Permeance and Membrane Rejection*. Although the PEG rejection values are not statistically significant when comparing the average of each rejection result, the incorporation of siloxene into the PES matrix caused an initial drop in the rejection, but increased as more siloxene was added. To reach a level again comparable to the base PES, likely due to the increased permeance (*3.3.1 Pure Water Permeance and Membrane Rejection*), initially offering less resistance to the PEG before the increased siloxene concentration began to aid rejection. The best performing PES-Siloxene membranes (0.150Si and 0.100Si) have circa 10 % rejection for 35,000 g mol^{-1}, 9 % rejection for the 10,000 g mol^{-1} PEG, and 7 % rejection for the 3000 g mol^{-1}. Both membranes containing PVP saw a decrease in the PEG rejection compared to their base counterpart.

Limitations of using the PEG method to assess the MWCO of membranes have been discussed in the literature [56,57]. Linear PEGs, coiled in solution, tend to unravel when passing through pores, resulting in an apparent lower MWCO than what is observed with other probe molecules. For instance, rejections above 99 % of dyes of MWs between 700 and 1400 g mol^{-1} have been obtained using PES membranes with a PEG MWCO of 4700 g mol^{-1} [56]. PEG MWCO 10–20 % lower than those of other molecules, e.g., trimethylolpropane ethoxylates have also been reported [57]. Nevertheless, the PEG MWCO in Fig. 4 can still distinguish rejection capacities between membranes, and although the absolute values may be underestimated, the results show consistent trends.

Table 2
Size analysis of the MMM sponge-like material and ratio of Macrovoids/Sponge-like material in the membrane cross-section.

Membrane	Sponge-like material	Macrovoids
	Mm	Macrovoids/sponge-like ratio
PES	0.079 (± 0.007)	0.507
3PVP	0.094 (± 0.006)	3.577
0.025Si	0.080 (± 0.003)	0.395
0.050Si	0.052 (± 0.002)	0.543
0.100Si	0.100 (± 0.014)	0.500
0.150Si	0.085 (± 0.005)	0.404
0.250Si	0.079 (± 0.002)	0.370
0.150Si_3PVP	0.091 (± 0.012)	1.739

3.2.2. *Membrane hydrophilicity & surface charge*

To evaluate the hydrophilicity of the membranes, contact angle measurements were carried out as displayed in Fig. 5a. The base PES membrane has a contact angle of 56° (±1°), while siloxene incorporated membranes (0.025Si - 0.250Si) exhibited lower contact angles. Membrane 0.150Si more than halved the water contact angle to 27° (±1°), demonstrating the substantial hydrophilic effect of the siloxene addition, due to increased hydrogen bonding. The addition of hydrophilic 2D nanomaterials has previously been shown to reduce the surface roughness of polymeric membranes, resulting in a lower water contact angle [25,58]. Increasing siloxene concentration from 0.150Si to 0.250Si displays a substantial increase in the contact angle, 27° (±1°) to 41° (±3°), respectively, reverting to a value similar to 0.025Si, of 48° (±4°). These data and previous trends support the formation of siloxene agglomerates, reducing its effectiveness [30]. Commercial PES Biomax® measured the highest contact angle of 62° (±2°) of all the measured membranes. Overall results show improvements in the hydrophilicity shown by the PES-Siloxene membranes over the fabricated and commercial PES membranes, which are ideal for facilitating water transport whilst reducing biofouling on the membrane's surface, as hydrophilicity reduces the aggregation of proteins on the membrane's surface [59].

When pore formers were added to the 3PVP membrane, a negligible change was observed compared to the base PES contact angle. However, when PVP was added to 0.150Si_3PVP, the contact angle increased to 46° (±1°), compared to its base comparison 0.150Si. Fig. 2 shows that the incorporation of PVP reduces the thickness of the skin layer of the asymmetric structure; therefore, there is less hydrophilic material at the surface of the membrane, which could cause a reduction in hydrophilicity [60]. In these instances, it would increase the membrane susceptibility to fouling from hydrophobic proteins, leading to a reduction in performance due to biofouling blocking membrane pores, reducing permeance and causing unwanted retention as materials get trapped in the fouling cake, making the membranes unfavourable for biomedical applications.

Fig. 5b shows that all of the fabricated membranes have a negative zeta potential, which in this instance is preferred as it repels negatively charged proteins, such as BSA and HSA, and attracts water molecules. There is a clear decrease in zeta potential upon the addition of siloxene to the MMMs. Base PES measured a value of −22.5 (± 0.1) mV compared to 0.150Si, which measured −35.4 (± 0.4) mV. This can be attributed to the presence of numerous polar Si-O-Si and OH groups in the siloxene nanosheets. Membrane 0.250Si, yet again, shows evidence of aggregation of siloxene due to the significant increase in the zeta potential, −25.8 (± 0.1) mV. Agglomeration reduces the number of functional groups available at the edges and surface of the siloxene sheets to affect the MMM. Furthermore, a direct correlation between the water contact angle and the zeta potential is evidenced. As the zeta potential decreases and the negative surface charge increases, the water contact angle

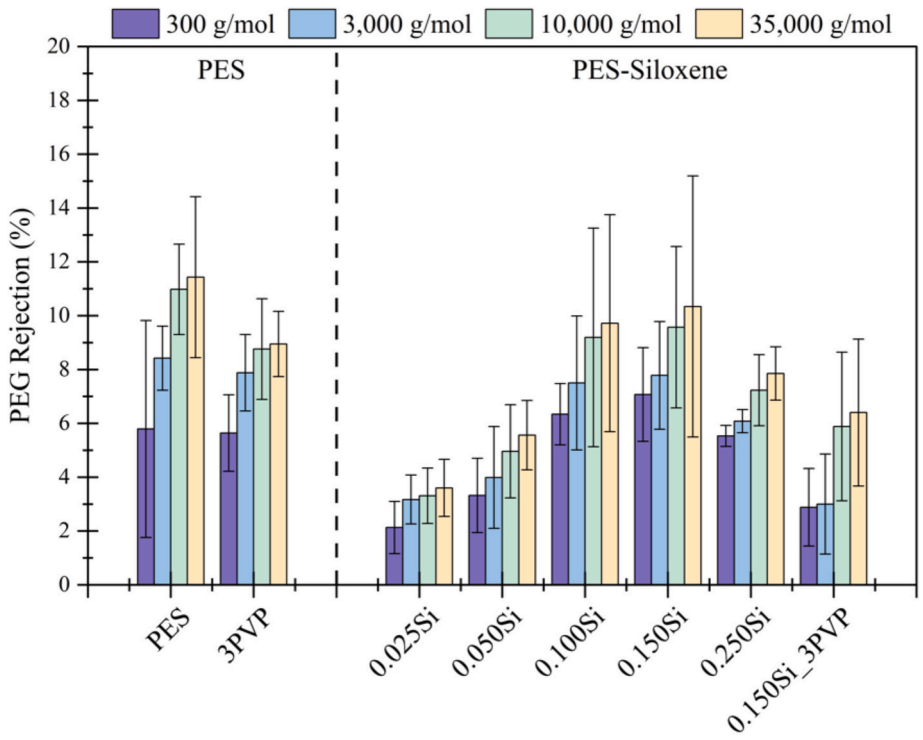

Fig. 4. Rejection (%) of polyethylene glycol (PEG) at four different molecular weights (300, 3000, 10,000, and 35,000 g mol^{-1}) in PES and PES-Siloxene membranes.

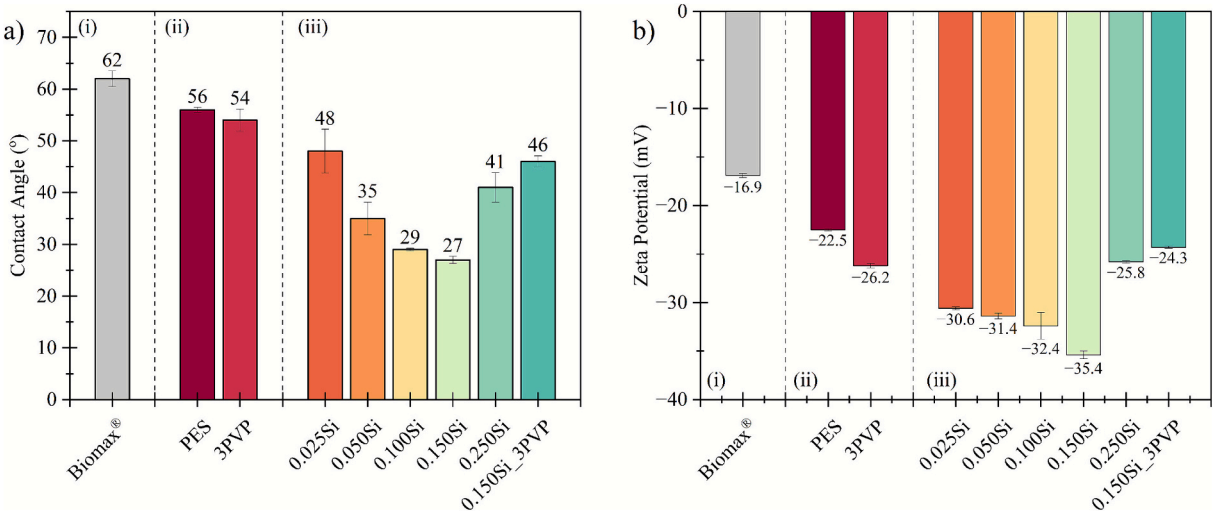

Fig. 5. a) Water Contact Angle (°) of (i) Commercial PES Biomax®, (ii) fabricated PES, and (iii) PES-Siloxene MMMs studied in this work. These were measured over ten seconds and averaged over three results using ultrapure water. b) Zeta potential values of (i) Commercial PES Biomax®, (ii) fabricated PES, and (iii) PES-Siloxene MMMs studied in this work. The measurements were taken using a streaming potential method with a KCl electrolyte solution (0.01 M), with a gap height of 100 μm and a pH of ~7.

decreases. The polar nature of the water molecules means they are attracted to polar surfaces, where hydrogen bonding can more readily occur and therefore result in a lower water contact angle. This could also potentially benefit the membrane performance, as the negatively charged surface will have a stronger attraction to water molecules and be more resistant to proteins. Resulting in potentially increased *PWP*, protein rejection and resistance.

3.3. Evaluation of membrane performance

3.3.1. Pure water permeance and membrane rejection

The addition of siloxene to the PES matrix caused the permeance to increase gradually, from 74.5 (± 10.5) LMHBar in the base PES membrane to 146.7 (± 14.2) LMHBar in membrane 0.150Si (Fig. 6a). The increase in water permeance is attributed to a combination of enhanced porosity, net surface negativity, increased hydrogen bonding between the water and PES-Siloxene matrix (Fig. 7a, Fig. 7c & Fig. 7e). Along with deeply penetrating macrovoids membranes caused by the addition of fillers to the PES, which facilitates surface diffusion of water through the membrane structure rather than absorption. Moreover, the addition of hydrophilic nanosheets to the casting solution will cause more rapid phase separation during membrane fabrication, making large pores and therefore allowing for a high permeance [19]. Commercial PES Biomax® membrane achieved a permeance of 118.6 (± 9.1) LMHBar,

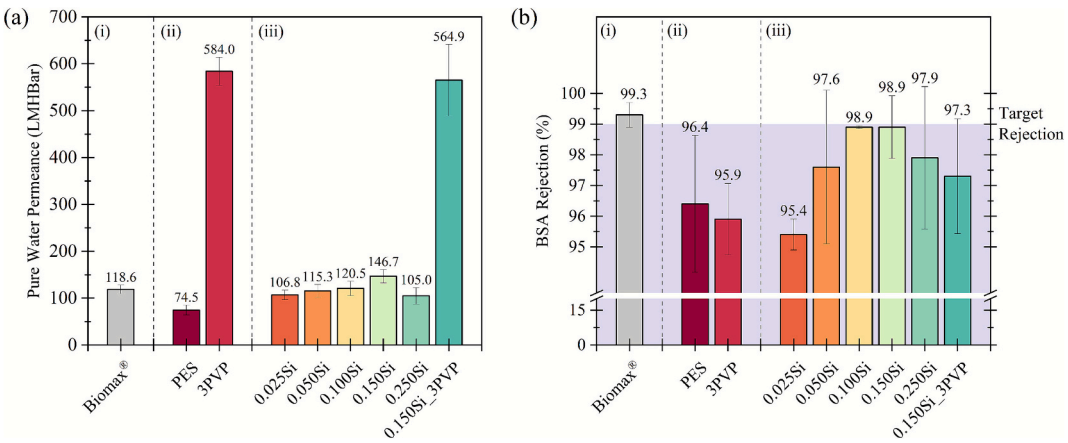

Fig. 6. (a) Pure Water Permeance (*PWP*, LMHBar) of (i) Commercial PES Biomax®, (ii) fabricated PES, and (iii) PES-Siloxene MMMs studied in this work. Measurements were made at 4 bar and continued until flux equilibration, using an effective area of 1.27 cm^2; **(b)** Rejection (%) of 80 g L^{-1} BSA of (i) Commercial PES Biomax®, (ii) fabricated PES, and (iii) PES-Siloxene MMMs studied in this work. UV–Vis spectroscopy at a wavelength of 280 nm was performed to assess the feed and permeate concentrations, which were then imputed to Eq.(3).

significantly outperforming the base PES membrane but only matching the lower 0.050Si siloxene concentrations in performance, resulting in a water permeance of PES-Siloxene membranes outperforming the commercial membrane Biomax® in most instances.

When PVP was introduced to the matrix, there was a significant increase in the water permeance. Membrane 3PVP increased the water permeance from 74.5 (± 10.5) to 584.0 (± 29.9) LMHBar, and 0.150Si_3PVP from 146.7 (± 14.2) to 564.9 (± 76.3) from LMHBar, when comparing to their respective counterpart membranes with no PVP, PES and 0.150Si. These data suggest that the PVP overwhelms the effect of the filler material, as there is no significant difference between the permeance of the two membranes. Permeance results can be explained by the tortuosity (τ) of the membrane morphology. Tortuosity has an inverse relationship with porosity, which can be estimated using, among others, the Bruggeman relation as per Eq. 9 [61].

$$\tau^2 = \varepsilon^{-1/2} \tag{9}$$

From this relationship, it can be said that the membranes with the highest porosity, particularly those with PVP additives, have a tortuosity close to unity, contributing to the observed high permeance. The remaining membranes would have increased tortuosity. While the large finger-like macrovoids are easy to navigate, the denser sponge-like material offers more resistance, causing the said increase. For instance, 0.150Si would have a lower tortuosity than PES due to the increased number and size of finger-like macrovoids in its morphology, which is supported by higher permeance and porosity. Moreover, the addition of 2D nanomaterials to polymeric matrices creates molecular transport channels in the interlayer spacing between the nanoflakes and the material. When the 2D nanomaterial is well dispersed, these channels shorten and therefore improve the overall membrane permeance [49,62], which can be seen in membrane 0.150Si. Moreover, the enhanced chain packing promoted by the siloxene, along with the interlayer spacing channels, simply makes a larger number of channels in a narrower space, helping to facilitate the enhanced permeance. Altogether, this further supports the siloxene agglomeration (poor dispersion) of membrane 0.250Si being the cause for the membrane's reduced performance; not only increasing transport pathlength but also increasing hydrophobicity and surface charge while decreasing porosity, making water transport more difficult compared to 0.150Si. The complete relationship between the porosity/hydrophilicity/surface charge and the permeance can be seen in Fig. 7.

As discussed previously, the target BSA rejection was 99 %, matching the benchmark of the commercial PES Biomax, which measured 99.3 % (± 0.4 %) BSA rejection in this study. PES is well known for being a capable UF membrane material for water treatment systems, with the base PES able to achieve a BSA rejection of 96.4 % (± 2.2 %) without the incorporation of any 2D nanomaterials [39,63]. Fig. 6b shows that increasing loadings of siloxene displayed an increase up to 98.9 % for both 0.100Si (± 1.1 %) and 0.150Si (± 2.2 %), to the 99 % threshold and within error and the Biomax®.

The increased rejection for the PES-Siloxene membranes compared to the base PES can be attributed to the increased surface negativity (−35.4 mV in 0.150Si) and subsequent hydrophilicity imparted by the incorporation of the 2D nanomaterial (Fig. 7d & Fig. 7f). The negatively charged membrane's surface generates electrostatic interactions and repels the hydrophobic exterior of the net negative BSA [64]. It is also well documented that high concentrations of proteins begin to aggregate and build up on the membrane's surface, particularly with relatively hydrophobic membranes, which can cause self-rejection of the proteins [65,66]. However, the hydrophilic material, like siloxene, incorporated in the membrane attracts the water due to the strongly favoured hydrogen bonding over the largely hydrophobic exterior of the protein (Fig. 7b and Fig. 7d). This, alongside the electrostatic repulsion, reduces the effectiveness of the mass transfer of the BSA and therefore the potential for cake formation [67,68]. If self-rejection of BSA was occurring, it would be expected that membranes 0.100Si and 0.150Si, with higher *PWP* and therefore larger pores, would have less BSA rejection than membranes like PES or 0.025Si. However, the opposite is seen, meaning it must be the electrostatic repulsion and hydrophilicity of the membrane itself that enhances the rejection. Moreover, the turbulence created by the stirrer inside the membrane module prevents further cake formation.

Compared to PES, 0.025Si shows a decrease in the BSA rejection to 95.4 % (± 0.5 %). The addition of 0.025 wt% Siloxene reduced the overall resistance to mass transfer, which increased water and BSA permeance. The continued addition of siloxene facilitated water transport and increased resistance to BSA. Moreover, 0.250Si also shows a reduction in the rejection from 0.150Si, likely as a result of the agglomeration of siloxene reducing its polar and hydrophilic effect, evident in the increased water contact angle (Fig. 5).

The addition of PVP caused the BSA rejection to drop in all three cases compared to their base counterparts. Although the increased porosity and permeance of these membranes can be very beneficial, in this instance, the ease of transport through the membrane limits the membrane's BSA rejection. Neither membrane 3PVP nor 0.150Si_3PVP have BSA rejection reaching 99 %, even those containing 2D nanomaterials at optimised concentrations. Therefore, in this given application, the use of PVP was less beneficial due to the reduction in BSA

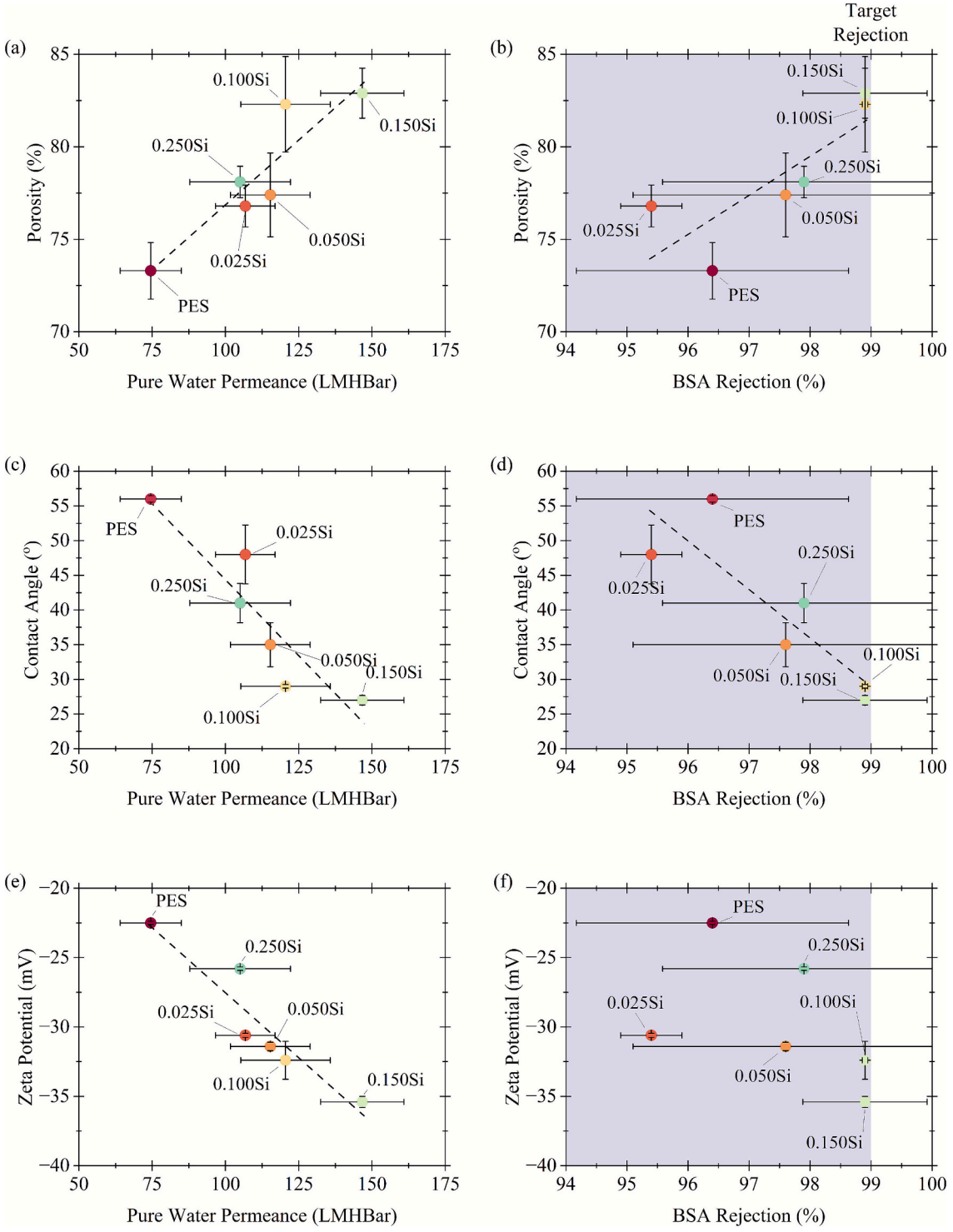

Fig. 7. Parity plots showing membrane performance vs characteristics correlations. Dashed lines correspond to linear regression line: **(a)** Porosity (%) vs Pure water permeance (*PWP*, LMHBar), $R^2 = 0.8351$; **(b)** Porosity (%) vs BSA Rejection (%), $R^2 = 0.6652$; **(c)** Contact angle (°) vs Pure water permeance (*PWP*, LMHBar), $R^2 = 0.8318$; **(d)** Contact angle (°) vs BSA Rejection (%), $R^2 = 0.7950$; **(e)** Zeta Potential (mV) vs Pure water permeance (*PWP*, LMHBar), $R^2 = 0.8802$; and **(f)** Zeta Potential (mV) vs BSA Rejection (%), $R^2 = 2507$.

rejection it generates.

3.3.2. *Antifouling properties*

Membranes used in biomedical applications are often only used a single time, due to the increased risk of blood infection and exposure to harmful germicides when membranes are sterilised [69]. However, despite being single-use, meaning they won't require cleaning for reuse, the membranes must still be fouling-resistant to ensure the membrane can maintain function while in use. The antifouling properties of Biomax®, PES, and 0.150Si were evaluated by calculating the *FRR*, R_t, R_r, and R_i, using Eqs. 5–8 and are presented in Fig. 8a. A long-term BSA permeation experiment was also carried out to support this further (Fig. 8b). These membranes were chosen to assess the antifouling performance of the PES-Siloxene membranes against the base PES

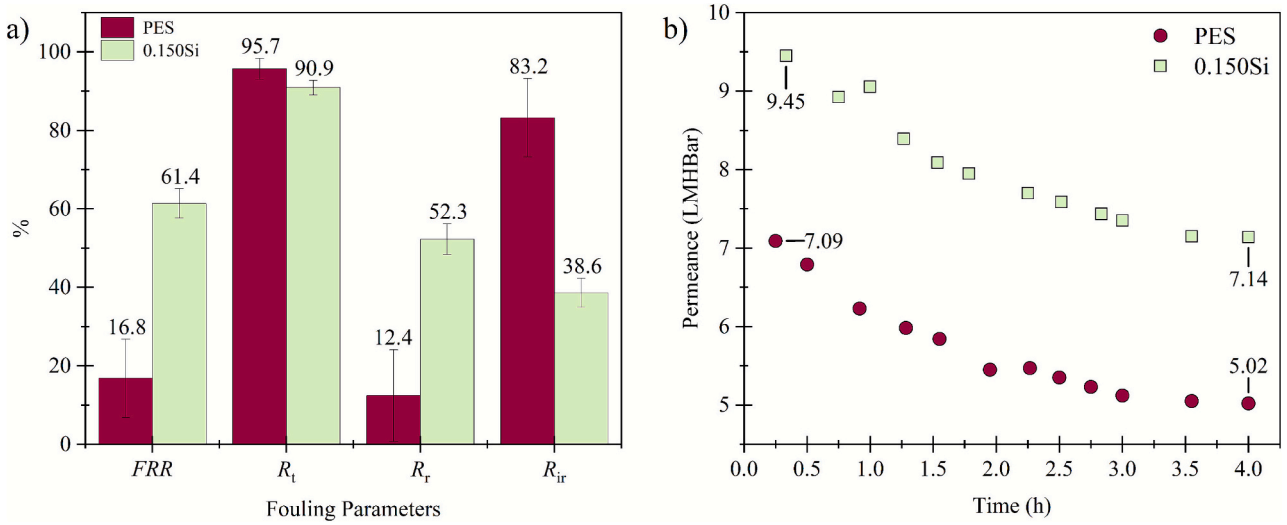

Fig. 8. (a) Flux recovery ratio (*FRR*), total flux decline ratio (R_t), reversible flux decline ratio (R_r), and irreversible flux decline ratio (R_{ir}), for membranes PES and 0.150Si, calculated using Eqs.(5, 6, 7), and (8), respectively. (b) Long-term BSA permeance for membranes PES and 0.150Si.

membrane. Membrane 0.150Si was ideal as it fits the necessary outlined criteria with high hydrophilicity, the largest negative zeta potential, improved permeance and BSA rejection ~99 %. 0.150Si was chosen over 0.100Si due to the equivalent BSA rejection and enhanced water permeance.

The addition of siloxene showed a substantial improvement to all parameters compared to PES, which can be attributed largely to the enhanced negative surface charge and hydrophilicity shown in the zeta potential and water contact angle measurements (Fig. 5). Membrane 0.150Si had an *FRR* of 61.4 % (± 3.7 %), respectively, whereas PES achieved just 16.8 % (± 10.0 %). In addition, it was expected that the R_t would be substantial due to the BSA being so abundant at high concentration; however, 0.150Si was able to maintain a higher percentage of its permeance, losing 90.9 % (± 1.9 %) of its original permeance, falling to ~14 LMHBar, whereas PES lost 95.7 % (± 3.7 %), only achieving an average permeance of ~3 LMHBar. 0.150Si was able to sustain a higher permeance while maintaining a BSA rejection of ~99 %, which is further illustrated in Fig. 8b. Long-term performance is important as it reflects performance in long-term applications such as hemofiltration or haemodialysis, which last between 3 and 4 h (according to NHS UK) [42]. R_r and R_{ir} for the membrane 0.150Si illustrate an increase in the R_r and a decrease in the R_{ir} in relation to the base PES membrane. The improved hydrophilicity will generate more favourable hydrogen bonding interactions at the surface of the membrane with the water in the solution compared to the BSA, reducing the deposition and, therefore, its adsorption to the surface and inside the pores of the membrane [70–72]. Moreover, the increased negativity of the membrane's surface further repels the net negative proteins, due to electrostatic repulsion, largely preventing the BSA from binding and agglomerating to the membrane [28,73–75]. It has also been shown that the addition of hydrophilic 2D nanomaterials can reduce the surface roughness of polymeric membranes, reducing the number of depressions on the membrane surface where foulants could be trapped [25,58]. From this, it is evident that the addition of the siloxene to the PES matrix significantly improves the membrane's antifouling performance.

As aforementioned, this test was also attempted with the commercial PES membrane Biomax®. However, difficulties were encountered when completing the test. The PWP_1 was calculated without issue, but when the membrane module was cleaned and feed solutions were changed to the concentrated BSA solution no permeation was observed, even after several hours of permeation testing. SEM images were taken of the Biomax® before and after testing (see Fig. S7 and S8). These showed densification at the membrane surface that may be responsible for restricting the mass transfer. After multiple attempts, it was determined that retesting these membranes, to complete J_{BSA} and PWP_1, was not possible. As a result, the antifouling test could not be completed. Despite this, given the high contact angle of the Biomax® and similar composition to fabricated PES, it could be inferred that the membrane would have similar antifouling performance.

The data in Fig. 8 show that the addition of the filler material makes the membranes more resistant to permanent fouling from the proteins in the solution compared to the base PES membranes, which will help maintain the membrane's improved performance in biomedical applications. Furthermore, the reduced fouling, paired with the enhanced permeance, would ensure that the membrane can provide the effective area, potentially reducing the area necessary for sufficient performance.

3.4. Comparison of PES-Siloxene and other PES-based MMM

Other 2D nanomaterials have also been used to improve membrane performance. Some recent membrane developments for BSA separation and antifouling found in other literature are listed in Table 3. GO and its derivatives are the most notable 2D nanofillers and have several positive impacts. While overall amphiphilic GO possesses many oxygenated functional groups, all of which are hydrophilic. Studies have shown that the addition of GO increased water affinity; hence, the permeance improved the antifouling properties of the membrane and maintained high protein rejection [20,76–78]. Consequently, GO has been considered a beneficial addition to haemodialysis PES membranes and has shown significant potential [21], whereas other 2D nanomaterials have limited use in membrane-based biomedical applications. In this line, previous work has shown PES MMM containing 0.1 wt% AGO that showed BSA rejection of 97 % and ~ 93.2 % upon the addition of 3 wt% pore-forming additive while having a permeance of 1.17 and 53.8 LMHBar, respectively [26]. However, this data lacked testing at high (80 g L^{-1}) BSA concentrations to match this study, as a more standard concentration of 1 g L^{-1} was used instead. Likewise, although all the membranes listed in Table 3 may have substantial antifouling properties (*FRR*), testing was completed with a very low BSA concentration, ranging from 0.10 to 1.00 g L^{-1}. In the present study, the PES-Siloxene membrane antifouling properties remain competitive with reported literature despite the BSA concentration being 80–800 times higher, while maintaining BSA rejection of circa 99 %.

The lack of information available where PES-Filler membranes are used at high BSA concentrations gives rise to the need for another base case using a 2D nanomaterial in a PES matrix to be provided for the PES-

Table 3
Selected recent works found in the literature on comparative membrane performance of mainly PES-based MMMs with added nanofillers using BSA-based feed systems.

Membrane	System	Performance	Ref.
PES/AGO	Pure water 1 g L^{-1} BSA	1.17 LMHBar ~97 % rejection ~65 % *FRR*	[26]
PES/AGO/PVP	Pure water 1 g L^{-1} BSA	53.8 LMHBar 93.2 % rejection	[26]
PES/GO	Pure water 1 g L^{-1} BSA	13 LMHBar ~96 % rejection ~60 % *FRR*	[78]
PES/GO/ Tetronic® T904	Pure water 1 g L^{-1} BSA	254 LMHBar ~93 % rejection ~59 % *FRR*	[78]
PES/O-MoS_2	Pure water 1 g L^{-1} BSA	75.2 LMHBar 88.2 % *FRR*	[79]
PES/GO/Fe_3O_4	Pure water 1 g L^{-1} BSA	~175 LMHBar 95 % rejection 87.9 % *FRR*	[80]
PSF/GO-guanidyl	Pure water 0.2 g L^{-1} BSA	204 LMHBar 95.1 % rejection 82.4 % *FRR*	[81]
PES/MoS2/O-MWCNTs/PVP	Pure water 0.5 g L^{-1} BSA	64 LMHBar 99 % rejection ~60 % *FRR*	[82]
PES/UiO-66-NH_2@CQDs	Pure water 1 g L^{-1} BSA	~272 LMHBar ~96 % rejection ~87 % *FRR*	[83]
PES/GO-SP	Pure water 0.5 g L^{-1} BSA	~3 LMHBar ~93 % *FRR*	[84]
PES/MDA/GO	Pure water 0.25 g L^{-1} BSA	12.7 LMHBar 70 % *FRR*	[85]
PES/AFBN	Pure water 0.25 g L^{-1} BSA	~57 LMHBar ~99 % rejection 90.4 % *FRR*	[86]
PES/WS_2	Pure water 0.25 g L^{-1} BSA	364 LMHBar 98 % rejection ~69 % *FRR*	[87]
PES/ *Z*-MXene	Pure water 0.1 g L^{-1} BSA	324 LMHBar ~97 % rejection ~97 % *FRR*	[88]
PES/ charcoal-NM	Pure water 0.1 g L^{-1} BSA	410 LMHBar ~95 % rejection ~95 % *FRR*	[89]
PES/Siloxene	Pure water 80 g L^{-1} BSA	146.7 LMHBar 98.8 % rejection 61.5 % *FRR*	This work

MWCNT – Multiwalled carbon nanotube; CQD – Carbon quantum dot; GO-SP – Photo-responsive graphene oxide-spiropyran; MDA – Melamine-based dendrimer amines; AFBN – Amine functionalised boron nitride; MXene - (Ti3C2Tx); charcoal-NM – Charcoal-nanomaterial.

Siloxene membranes to confirm if the siloxene is providing a significant difference over the other nanomaterials in the literature. Therefore, AGO was chosen at 0.1 wt% to be fabricated and evaluated as a comparative material to the siloxene in a PES matrix, due to its current antifouling performance in the literature and GO's emergence into the biomedical research within membrane applications [21,22]. 2D nanomaterial characterisation can be found in Supporting Information (Fig. S3 and S4). Identical PES-based casting solutions were prepared as per Luque-Alled et al. [26], resulting in the fabrication of membranes named here as 0.100AGO and 0.100AGO_3PVP. These membranes were characterised and tested using the same methodologies as the rest of this work (Table 4). Results can be found in Table S3, Fig. S9, and Fig. S10 in the Supporting Information. Some differences between the permeance and porosity of the fabricated and reported PES-AGO membranes were observed. These differences have been discussed in full in the Supporting Information (*6. Characterisation of PES-AGO Membranes*).

The fabricated PES-Siloxene membranes herein outperform AGO-based membranes, with enhanced hydrophilicity, *PWP*, and antifouling performance. It was observed that the 0.100AGO and

Table 4
Comparison between PES-Siloxene and PES-AGO membranes.

Membrane	0.100AGO	0.150Si	0.100AGO_3PVP	0.150Si_3PVP
Contact angle / °	47 (± 1)	27 (± 1)	49 (± 1)	46 (± 1)
Zeta potential / mV	−25.7 (± 0.0)	−35.4 (± 0.4)	−25.1 (± 1.3)	−24.3 (± 0.1)
PWP / LMHBar	115.8 (± 11.7)	146.7 (± 14.2)	593.0 (± 14.3)	564.9 (± 76.3)
BSA rejection / %	99.3 (± 0.2)	98.9 (± 2.2)	94.8 (± 1.0)	97.3 (± 1.8)
FRR / %	51.8 (± 1.9)	61.4 (± 3.7)	N/A	N/A

0.100AGO_3PVP had similar surface and cross-sectional morphology to the PES-Siloxene and 0.150Si_3PVP, respectively. Moreover, 0.100AGO achieved comparable permeance to 0.050Si and 0.100Si but significantly less than 0.150Si while maintaining ~99 % BSA rejection and low PEG rejection. In contrast, membrane 0.100AGO_3PVP had similar performance to 0.150Si_3PVP membranes, again suggesting that the addition of PVP dominated the performance, as both membranes had statistically comparable permeance and BSA rejection. Interestingly, the addition of hydrophilic AGO did not decrease the contact angle or zeta potential as much as the addition of siloxene, only reaching 47° (±1°) and − 25.7 mV, respectively, for 0.100AGO; similar to low siloxene concentrations. The cause of this could be the high surface area of the siloxene sheet due to the corrugated structure [31], allowing for more favourable interactions with approaching water molecules. Furthermore, the fouling properties of 0.100AGO were also assessed (see Table 4 and Fig. S11) using the high BSA feed concentration. The *FRR* of 0.100AGO fell short of the 0.150Si, reaching just 51.8 % compared to 61.4 %. Despite AGO having been shown to have potential as a filler in this membrane application, based on the observations in this study, siloxene is a better choice due to improvements to all parameters assessed in this work.

It is interesting to note that the PES-AGO membranes fabricated for this report had a permeance and porosity significantly higher than that reported in the original article [26]. A complete discussion of this observation can be found in the Supporting Information (*6. Characterisation of PES-AGO Membranes*), to not draw focus from the main article.

4. Conclusions

Siloxene was successfully synthesised and incorporated into PES-based MMMs. We demonstrate the use of siloxene in PES to study the antifouling properties of the membranes, with results showing that 0.15 wt% imparted a favoured loading to the performance. The addition of the easy-to-synthesise 2D siloxene showed a significant enhancement in the negative surface charge of the membrane, reaching a zeta potential of −35.4 (± 0.4) mV for 0.150Si compared to −22.5 (± 0.1) mV for base PES. This resulted in a large improvement in the membrane's hydrophilicity, reducing the water contact angle from 52° (±1°) for base PES to 27° (±1°) for 0.150Si. The base PES membrane fell short of the ~99 % protein rejection target, whereas the addition of siloxene at 0.150 wt% (0.150Si) and 0.100 wt% (0.100Si) enhanced this to ~99 %. Furthermore, these membranes overcame the trade-off between permeance and protein selectivity, with membrane 0.150Si having approximately double the permeance of PES, 146.7 (± 14.2), to 74.5 LMHBar, while maintaining higher rejection. Building on this, due to the heightened surface negativity, enhanced hydrophilicity, higher permeance and protein rejection. The PES-Siloxene membrane was also more capable of withstanding larger protein concentrations while maintaining performance. The recovered flux (*FRR*) after protein fouling increased from only 16.8 % for the base PES membrane to 61.4 % for the 0.150Si membrane, showing a significant improvement in permeant protein resistance. It was also determined that the addition of PVP pore formers

wasn't beneficial to this application, despite improving the water permeance significantly. Furthermore, membrane 0.150Si outperformed the commercial PES Biomax® and PES-AGO membranes in every respect, showing its enhancement on current benchmarks.

Altogether, the PES-Siloxene membranes, particularly 0.150Si, exhibit great potential to be used within biomedical devices, with almost complete albumin retention at realistic concentrations, UF water permeance, significant resistance to biological fouling, and greater performance than other currently available commercial alternatives. The next step in this project is to move closer to genuine conditions and their impact on the membranes by simulating more complex environments with multiple foulants, before moving to blood plasma and whole blood samples. Development of biomedical technologies, such as haemodialysis, hemofiltration, and biosensing pre-treatment, as well as other biological purifications, will benefit from the use of siloxene in their separation stages to ensure the material's long-term suitability and process feasibility.

Acknowledgements

The authors would like to thank the SynHiSel EPSRC Programme Grant EP/V047078/1 for funding this project.

CRediT authorship contribution statement

Benjamin Stewart Moore: Writing – original draft, Visualization, Validation, Methodology, Formal analysis, Data curation, Conceptualization. **Pablo López-Porfiri:** Writing – review & editing, Methodology, Investigation, Formal analysis, Conceptualization. **Dinesh K. Mahalingam:** Writing – review & editing, Investigation. **Elliot Craddock:** Methodology, Investigation. **Abdullah Albiladi:** Methodology, Investigation. **Carmine D'Agostino:** Supervision. **John Chew:** Writing – review & editing, Supervision, Resources, Project administration, Funding acquisition. **Davide Mattia:** Writing – review & editing, Supervision, Resources, Project administration, Investigation, Funding acquisition. **Patricia Gorgojo:** Writing – review & editing, Supervision, Conceptualization. **María Pérez-Page:** Writing – review & editing, Supervision, Resources, Project administration, Methodology, Funding acquisition, Conceptualization.

Declaration of competing interest

The authors declare that they have no known competing financial interests or personal relationships that could have appeared to influence the work reported in this paper.

Appendix A. Supplementary data

Supplementary data to this article can be found online at https://doi.org/10.1016/j.seppur.2026.136740.

Data availability

Data will be made available on request.

References

[1] E.R. Radu, S.I. Voicu, V.K. Thakur, Polymeric membranes for biomedical applications, Polym. (Basel). 15 (2023) 619, https://doi.org/10.3390/polym15030619.
[2] X. Chen, J. Li, Bioinspired by cell membranes: functional polymeric materials for biomedical applications, Mater. Chem. Front. 4 (2020) 750–774, https://doi.org/10.1039/c9qm00717b.
[3] N. Tolkoff-Rubin, Treatment of Irreversible Renal Failure, Twenty Fou, Elsevier Inc, 2012, https://doi.org/10.1016/B978-1-4377-1604-7.00133-0.
[4] A. Shiohara, B. Prieto-Simon, N.H. Voelcker, Porous polymeric membranes: fabrication techniques and biomedical applications, J. Mater. Chem. B 9 (2021) 2129–2154, https://doi.org/10.1039/d0tb01727b.
[5] Q. Xie, S. Zhang, Z. Xiao, X. Hu, Z. Hong, R. Yi, W. Shao, Q. Wang, Preparation and characterization of novel alkali-resistant nanofiltration membranes with enhanced permeation and antifouling properties: the effects of functionalized graphene nanosheets, RSC Adv. 7 (2017) 18755–18764, https://doi.org/10.1039/c7ra00928c.
[6] M. Casciola, A. Donnadio, M. Pica, 3.7 Basic Aspects in Proton-Conducting Membranes for Fuel Cells, Elsevier Ltd., 2017, https://doi.org/10.1016/b978-0-12-409547-2.12259-0.
[7] H. Wang, T. Yu, C. Zhao, Q. Du, Improvement of hydrophilicity and blood compatibility on polyethersulfone membrane by adding polyvinylpyrrolidone, Fibers Polym. 10 (2009) 1–5, https://doi.org/10.1007/s12221-009-0001-4.
[8] C.J.O. Bacal, C.J. Munro, B. Tardy, J.W. Maina, J.A. Sharp, J.M. Razal, G. W. Greene, H.H. Nandurkar, K.M. Dwyer, L.F. Dumée, Fouling during hemodialysis – influence of module design and membrane surface chemistry, Adv. Membr. 4 (2024), https://doi.org/10.1016/j.advmem.2024.100100.
[9] K. Hiwatari, M. Yamamoto, K. Hayama, M. Kohori, F. Sakai, Evaluation of local membrane fouling in hemodialyzer, ASAIO J. 50 (2004) 177.
[10] H.J. Tanudjaja, A. Anantharaman, A.Q.Q. Ng, Y. Ma, M.B. Tanis-Kanbur, A. L. Zydney, J.W. Chew, A review of membrane fouling by proteins in ultrafiltration and microfiltration, J. Water Process Eng. 50 (2022) 103294, https://doi.org/10.1016/j.jwpe.2022.103294.
[11] M. Gryta, P. Woźniak, Polyethersulfone membrane fouling mitigation during ultrafiltration of wastewaters from car washes, Desalination 574 (2024) 117254, https://doi.org/10.1016/j.desal.2023.117254.
[12] X. Wen, C. He, Y. Hai, R. Ma, J. Sun, X. Yang, Y. Qi, H. Wei, J. Chen, Fabrication of an antifouling PES ultrafiltration membrane: via blending SPSF, RSC Adv. 12 (2022) 1460–1470, https://doi.org/10.1039/d1ra06354e.
[13] A. Blanco, G. Blanco, Medical biochemistry, in: A. Blanco, G. Blanco (Eds.), Med. Biochem., Second, Academic Press, 2022, pp. 21–75, https://doi.org/10.1016/B978-0-323-91599-1.00004-3.
[14] A. Murali, G. Lokhande, K.A. Deo, A. Brokesh, A.K. Gaharwar, Emerging 2D nanomaterials for biomedical applications, Mater. Today 50 (2021) 276–302, https://doi.org/10.1016/j.mattod.2021.04.020.
[15] J. Ouyang, S. Rao, R. Liu, L. Wang, W. Chen, W. Tao, N. Kong, 2D materials-based nanomedicine: from discovery to applications, Adv. Drug Deliv. Rev. 185 (2022) 114268, https://doi.org/10.1016/j.addr.2022.114268.
[16] X. Zhao, R. Zhang, Y. Liu, M. He, Y. Su, C. Gao, Z. Jiang, Antifouling membrane surface construction: Chemistry plays a critical role, J. Membr. Sci. 551 (2018) 145–171, https://doi.org/10.1016/j.memsci.2018.01.039.
[17] X. Li, A. Sotto, J. Li, B. Van der Bruggen, Progress and perspectives for synthesis of sustainable antifouling composite membranes containing in situ generated nanoparticles, J. Membr. Sci. 524 (2017) 502–528, https://doi.org/10.1016/j.memsci.2016.11.040.
[18] E. Yi, H.S. Kang, S.M. Lim, H.J. Heo, D. Han, J.F. Kim, A. Park, D.H. Choi, Y.I. Park, H. Park, Y.H. Cho, E.H. Sohn, Superamphiphobic blood-repellent surface modification of porous fluoropolymer membranes for blood oxygenation applications, J. Membr. Sci. 648 (2022) 120363, https://doi.org/10.1016/j.memsci.2022.120363.
[19] S. Mohsenpour, S. Leaper, J. Shokri, M. Alberto, P. Gorgojo, Effect of graphene oxide in the formation of polymeric asymmetric membranes via phase inversion, J. Membr. Sci. 641 (2022) 119924, https://doi.org/10.1016/j.memsci.2021.119924.
[20] M. Alberto, J.M. Luque-Alled, L. Gao, M. Iliut, E. Prestat, L. Newman, S.J. Haigh, A. Vijayaraghavan, P.M. Budd, P. Gorgojo, Enhanced organophilic separations with mixed matrix membranes of polymers of intrinsic microporosity and graphene-like fillers, J. Memb. Sci. 526 (2017) 437–449, https://doi.org/10.1016/j.memsci.2016.12.061.
[21] M.Z. Fahmi, M. Wathoniyyah, M. Khasanah, Y. Rahardjo, S. Wafiroh, Abdulloh, Incorporation of graphene oxide in polyethersulfone mixed matrix membranes to enhance hemodialysis membrane performance, RSC Adv. 8 (2018) 931–937, https://doi.org/10.1039/c7ra11247e.
[22] R.P. Rode, H.H. Chung, H.N. Miller, T.R. Gaborski, S. Moghaddam, Trilayer interlinked graphene oxide membrane for wearable hemodialyzer, Adv. Mater. Interfaces 8 (2021) 1–8, https://doi.org/10.1002/admi.202001985.
[23] A. Abdel-karim, J.M. Luque-alled, S. Leaper, M. Alberto, X. Fan, A. Vijayaraghavan, T.A. Gad-allah, A.S. El-kalliny, G. Szekely, S.I.A. Ahmed, S.M. Holmes, P. Gorgojo, PVDF membranes containing reduced graphene oxide : E ff ect of degree of reduction on membrane distillation performance, Desalination 452 (2019) 196–207, https://doi.org/10.1016/j.desal.2018.11.014.
[24] S. Leaper, A. Abdel-Karim, B. Faki, J.M. Luque-Alled, M. Alberto, A. Vijayaraghavan, S.M. Holmes, G. Szekely, M.I. Badawy, N. Shokri, P. Gorgojo, Flux-enhanced PVDF mixed matrix membranes incorporating APTS-functionalized graphene oxide for membrane distillation, J. Membr. Sci. 554 (2018) 309–323, https://doi.org/10.1016/j.memsci.2018.03.013.
[25] Z. Xu, J. Zhang, M. Shan, Y. Li, B. Li, J. Niu, B. Zhou, X. Qian, Organosilane-functionalized graphene oxide for enhanced antifouling and mechanical properties of polyvinylidene fluoride ultrafiltration membranes, J. Membr. Sci. 458 (2014) 1–13, https://doi.org/10.1016/j.memsci.2014.01.050.
[26] J.M. Luque-Alled, A. Abdel-Karim, M. Alberto, S. Leaper, M. Perez-Page, K. Huang, A. Vijayaraghavan, A.S. El-Kalliny, S.M. Holmes, P. Gorgojo, Polyethersulfone membranes: from ultrafiltration to nanofiltration via the incorporation of APTS functionalized-graphene oxide, Sep. Purif. Technol. 230 (2020) 115836, https://doi.org/10.1016/j.seppur.2019.115836.
[27] S. Sarkar, S. Kundu, Protein (BSA) adsorption on hydrophilic and hydrophobic surfaces, Mater. Today Proc. (2023), https://doi.org/10.1016/j.matpr.2023.04.200.

[28] S. Srinivasan, P.N. Sawyer, Role of surface charge of the blood vessel wall, blood cells, and prosthetic materials in intravascular thrombosis, J. Colloid Interface Sci. 32 (1970) 456–463, https://doi.org/10.1016/0021-9797(70)90131-1.
[29] A. Modi, S.K. Verma, J. Bellare, Graphene oxide-doping improves the biocompatibility and separation performance of polyethersulfone hollow fiber membranes for bioartificial kidney application, J. Colloid Interface Sci. 514 (2018) 750–759, https://doi.org/10.1016/j.jcis.2017.12.044.
[30] J. Ji, S. Mazinani, E. Ahmed, Y.M. John Chew, D. Mattia, Hydrophobic poly (vinylidene fluoride) / siloxene nanofiltration membranes, J. Membr. Sci. 635 (2021) 119447, https://doi.org/10.1016/j.memsci.2021.119447.
[31] P. Pazhamalai, K. Krishnamoorthy, S. Sahoo, V.K. Mariappan, S.J. Kim, Understanding the thermal treatment effect of two-dimensional siloxene sheets and the origin of superior electrochemical energy storage performances, ACS Appl. Mater. Interfaces 11 (2019) 624–633, https://doi.org/10.1021/acsami.8b15323.
[32] K. Krishnamoorthy, P. Pazhamalai, S.J. Kim, Two-dimensional siloxene nanosheets: Novel high-performance supercapacitor electrode materials, Energy Environ. Sci. 11 (2018) 1595–1602, https://doi.org/10.1039/c8ee00160j.
[33] C. Jia, F. Zhang, N. Zhang, Q. Li, X. He, J. Sun, R. Jiang, Z. Lei, Z.H. Liu, Bifunctional photoassisted Li-O_2 battery with ultrahigh rate-cycling performance based on siloxene size regulation, ACS Nano 17 (2023) 1713–1722, https://doi.org/10.1021/acsnano.2c12025.
[34] N. Deepak, S. Shukla, S. Saxena, Two-dimensional reduced siloxene metal-free semiconductor for enhanced photocatalytic performance, MRS Adv. 9 (2024) 590–595, https://doi.org/10.1557/s43580-024-00870-9.
[35] E. Magill, S. Demartis, E. Gavini, A.D. Permana, R.R.S. Thakur, M.F. Adrianto, D. Waite, K. Glover, C.J. Picco, A. Korelidou, U. Detamornrat, L.K. Vora, L. Li, Q. K. Anjani, R.F. Donnelly, J. Domínguez-Robles, E. Larrañeta, Solid implantable devices for sustained drug delivery, Adv. Drug Deliv. Rev. 199 (2023) 114950, https://doi.org/10.1016/j.addr.2023.114950.
[36] C. Zweigart, A. Boschetti-de-Fierro, M. Hulko, L.G. Nilsson, W. Beck, M. Storr, B. Krause, Medium cut-off membranes - closer to the natural kidney removal function, Int. J. Artif. Organs 40 (2017) 328–334, https://doi.org/10.5301/ijao.5000603.
[37] L. Torrijos-Morán, B.D. Lisboa, M. Soler, L.M. Lechuga, J. García-Rupérez, Integrated optical bimodal waveguide biosensors: principles and applications, Results Opt. 9 (2022) 100285.
[38] C.S. Huertas, D. Fariña, L.M. Lechuga, Direct and label-free quantification of MicroRNA-181a at attomolar level in complex media using a nanophotonic biosensor, ACS Sens. 1 (2016) 748–756, https://doi.org/10.1021/acssensors.6b00162.
[39] X. Li, X. Fang, R. Pang, J. Li, X. Sun, J. Shen, W. Han, L. Wang, Self-assembly of TiO_2 nanoparticles around the pores of PES ultrafiltration membrane for mitigating organic fouling, J. Membr. Sci. 467 (2014) 226–235, https://doi.org/10.1016/j.memsci.2014.05.036.
[40] P. López-Porfiri, P. Gavagni, B.S. Moore, M. González-Miquel, P. Gorgojo, M. C. Ferrari, M. Pérez-Page, The hydrophilic nature trade-off of supported ionic liquid membranes on CO_2/CH_4 separation performance, J. Mater. Chem. A 13 (2025) 13518–13531, https://doi.org/10.1039/d5ta00917k.
[41] R. Maier, M.R. Fries, C. Buchholz, F. Zhang, F. Schreiber, Human versus bovine serum albumin: a subtle difference in hydrophobicity leads to large differences in bulk and Interface behavior, Cryst. Growth Des. 21 (2021) 5451–5459, https://doi.org/10.1021/acs.cgd.1c00730.
[42] Dialysis - NHS, NHS, https://111.wales.nhs.uk/dialysis, 2025. (Accessed 22 December 2025).
[43] R.W. Baker, Membrane technology and applications, John Wiley & Sons, Ltd, 2010. https://doi.org/10.1016/C2009-0-19129-8.
[44] B.D. McCloskey, H.B. Park, H. Ju, B.W. Rowe, D.J. Miller, B.D. Freeman, A bioinspired fouling-resistant surface modification for water purification membranes, J. Membr. Sci. 413–414 (2012) 82–90, https://doi.org/10.1016/j.memsci.2012.04.021.
[45] Y. Wu, J. Zeng, Y. Zeng, H. Zhou, G. Liu, J. Jian, J. Ding, Polyethersulfone-polyvinylpyrrolidone composite membranes: Effects of polyvinylpyrrolidone content and polydopamine coating on membrane morphology, structure and performances, Chin. J. Chem. Eng. 38 (2021) 84–97, https://doi.org/10.1016/j.cjche.2020.09.012.
[46] J. Wu, Z. Wang, W. Yan, Y. Wang, J. Wang, S. Wang, Improving the hydrophilicity and fouling resistance of RO membranes by surface immobilization of PVP based on a metal-polyphenol precursor layer, J. Membr. Sci. 496 (2015) 58–69, https://doi.org/10.1016/j.memsci.2015.08.044.
[47] D.J. Seader, E.J. Henley, Chapter 14 Membrane Separations, 2nd ed, John Wiley & Sons, Inc, 2006, https://doi.org/10.5860/choice.36-5112.
[48] T. Miyano, T. Matsuura, S. Sourirajan, Effect of polivinylpyrrolidone additive on the pore size and the pore size distribution of polyethersulfone (victrex) membranes, Chem. Eng. Commun. 119 (1993) 23–39, https://doi.org/10.1080/00986449308936105.
[49] T. Yuan, L. Sarkisov, How 2D Nanoflakes improve transport in mixed matrix membranes: insights from a simple lattice model and dynamic mean field theory, ACS Appl. Mater. Interfaces 16 (2024) 8184–8195, https://doi.org/10.1021/acsami.4c00661.
[50] D. Al-Araji, F. Al-Ani, Q. Alsalhy, The permeation and separation characteristics of polymeric membranes incorporated with nanoparticles for dye removal and interaction mechanisms between polymer and nanoparticles: A Mini review, Eng. Technol. J. 40 (2022) 1399–1411, https://doi.org/10.30684/etj.2022.132572.1129.
[51] E. Craddock, R.M. Cuéllar-Franca, M. Pérez-Page, The incorporation of 2D materials into membranes to improve the environmental sustainability of vanadium redox flow batteries (VRFBs): A critical review, Curr. Opin. Chem. Eng. 40 (2023) 100906, https://doi.org/10.1016/j.coche.2023.100906.
[52] Z.X. Low, J. Ji, D. Blumenstock, Y.M. Chew, D. Wolverson, D. Mattia, Fouling resistant 2D boron nitride nanosheet – PES nanofiltration membranes, J. Membr. Sci. 563 (2018) 949–956, https://doi.org/10.1016/j.memsci.2018.07.003.
[53] W. Shao, S. Wu, Z. Hong, Q. Wang, Y. Xiong, R. Yi, Q. Xie, Z. Xiao, Preparation and characterization of asymmetric polyethersulfone nanofiltration membranes: the effects of polyvinylpyrrolidone molecular weights and concentrations, J. Appl. Polym. Sci. 133 (2016) 1–9, https://doi.org/10.1002/app.43769.
[54] D. Dolar, K. Košutić, Removal of pharmaceuticals by ultrafiltration (UF), nanofiltration (NF), and reverse osmosis (RO), Anal. Removal, Eff. Risk Pharm. Water Cycle (2013) 319–344, https://doi.org/10.1016/B978-0-444-62657-8.00010-0.
[55] M. Park, S.A. Snyder, Attenuation of contaminants of emerging concerns by nanofiltration membrane: Rejection mechanism and application in water reuse, in: Contam. Emerg. Concern Water Wastewater Adv. Treat. Process, Elsevier Inc, 2020, pp. 177–206, https://doi.org/10.1016/B978-0-12-813561-7.00006-7.
[56] J. Lin, W. Ye, M.C. Baltaru, Y.P. Tang, N.J. Bernstein, P. Gao, S. Balta, M. Vlad, A. Volodin, A. Sotto, P. Luis, A.L. Zydney, B. Van der Bruggen, Tight ultrafiltration membranes for enhanced separation of dyes and Na_2SO_4 during textile wastewater treatment, J. Membr. Sci. 514 (2016) 217–228, https://doi.org/10.1016/j.memsci.2016.04.057.
[57] A. Yushkin, R. Borisov, V. Volkov, A. Volkov, Improvement of MWCO determination by using branched PEGs and MALDI method, Sep. Purif. Technol. 211 (2019) 108–116, https://doi.org/10.1016/j.seppur.2018.09.043.
[58] J. Peng, Y. Su, Q. Shi, W. Chen, Z. Jiang, Protein fouling resistant membrane prepared by amphiphilic pegylated polyethersulfone, Bioresour. Technol. 102 (2011) 2289–2295, https://doi.org/10.1016/j.biortech.2010.10.045.
[59] R. Castellanos Espinoza, M.J. Huhn Ibarra, A.J. Montes Luna, M. Aguilar-Vega, M. M. Hernández Orozco, G. Luna Bárcenas, L.A. Baldenegro Pérez, M. Guerra Balcázar, B.L., España Sánchez, combined antibacterial and antifouling properties of polyethersulfone mixed matrix membranes with zwitterionic graphene oxide nanostructures, Polym. Eng. Sci. (2024) 1–11, https://doi.org/10.1002/pen.26825.
[60] M. Xiao, F. Yang, S. Im, D.S. Dlamini, D. Jassby, S. Mahendra, R. Honda, E.M. V. Hoek, Characterizing surface porosity of porous membranes via contact angle measurements, J. Membr. Sci. Lett. 2 (2022) 100022, https://doi.org/10.1016/j.memlet.2022.100022.
[61] L. Holzer, P. Marmet, M. Fingerle, A. Wiegmann, M. Neumann, V. Schmidt, Tortuosity and microstructure effects in porous media, 2023, https://doi.org/10.1007/978-3-031-30477-4.
[62] Z. Zhu, S. Wang, F. Pan, Z. Jiang, 2D-materials mixed-matrix membranes, in: G. Liu, W. Jin (Eds.), Two-Dimensional-Materials-Based Membr. Prep. Charact. Appl, 1st ed, WILEY-VCH GmbH, 2022, pp. 279–311.
[63] A. Abdel-Karim, H. Elhaes, A.S. El-Kalliny, M.I. Badawy, M. Ibrahim, T.A. Gad-Allah, Probing protein rejection behavior of blended PES-based flat-sheet ultrafiltration membranes: a density functional theory (DFT) study, Spectrochim. Acta A Mol. Biomol. Spectrosc. 238 (2020) 118399, https://doi.org/10.1016/j.saa.2020.118399.
[64] E. Suryawirawan, A.E.M. Janssen, R.M. Boom, Bovine serum albumin rejection by an open ultrafiltration membrane : characterization and modeling, Memb. (Basel). 14 (2024) 26.
[65] E. Iritani, N. Katagiri, Y. Ishikawa, D.Q. Cao, Cake formation and particle rejection in microfiltration of binary mixtures of particles with two different sizes, Sep. Purif. Technol. 123 (2014) 214–220, https://doi.org/10.1016/j.seppur.2013.12.033.
[66] M. Pinelo, C. Ferrer, A.S. Meyer, G. Jonsson, Controlling the rejection of protein during membrane filtration by adding selected polyelectrolytes, Sep. Purif. Technol. 85 (2012) 54–60, https://doi.org/10.1016/j.seppur.2011.09.039.
[67] P. Wang, J. Meng, M. Xu, T. Yuan, N. Yang, T. Sun, Y. Zhang, X. Feng, B. Cheng, A simple but efficient zwitterionization method towards cellulose membrane with superior antifouling property and biocompatibility, J. Membr. Sci. 492 (2015) 547–558, https://doi.org/10.1016/j.memsci.2015.06.024.
[68] L.J. Zhu, F. Liu, X.M. Yu, A.L. Gao, L.X. Xue, Surface zwitterionization of hemocompatible poly(lactic acid) membranes for hemodiafiltration, J. Membr. Sci. 475 (2015) 469–479, https://doi.org/10.1016/j.memsci.2014.11.004.
[69] A. Upadhyay, B.L. Jaber, Reuse and biocompatibility of hemodialysis membranes: clinically relevant? Semin. Dial. 30 (2017) 121–124, https://doi.org/10.1111/sdi.12574.
[70] Y.F. Zhao, L.P. Zhu, Z. Yi, B.K. Zhu, Y.Y. Xu, Zwitterionic hydrogel thin films as antifouling surface layers of polyethersulfone ultrafiltration membranes anchored via reactive copolymer additive, J. Membr. Sci. 470 (2014) 148–158, https://doi.org/10.1016/j.memsci.2014.07.023.
[71] Q. Xue, H. Cao, F. Meng, M. Quan, Y.K. Gong, Cell membrane mimetic coating immobilized by mussel-inspired adhesion on commercial ultrafiltration membrane to enhance antifouling performance, J. Membr. Sci. 528 (2017) 1–11, https://doi.org/10.1016/j.memsci.2017.01.009.
[72] D.I. Petukhov, D.J. Johnson, Membrane modification with carbon nanomaterials for fouling mitigation: A review, Adv. Colloid Interf. Sci. 327 (2024) 103140, https://doi.org/10.1016/j.cis.2024.103140.
[73] H.P. Fernandes, C.L. Cesar, M. de L. Barjas-Castro, Electrical properties of the red blood cell membrane and immunohematological investigation, Rev. Bras. Hematol. Hemoter. 33 (2011) 297–301, https://doi.org/10.5581/1516-8484.20110080.
[74] Q. Lin, X. Chen, X. Zheng, Z. Yang, Y. Xiang, C.Y. Tang, S. Yi, G. Zeng, J. Luo, Electrostatically enhanced surface segregation boosts anti-fouling performance of mixed matrix membranes, J. Membr. Sci. 725 (2025) 124036, https://doi.org/10.1016/j.memsci.2025.124036.

[75] H. Mo, K.G. Tay, H.Y. Ng, Fouling of reverse osmosis membrane by protein (BSA): Effects of pH, calcium, magnesium, ionic strength and temperature, J. Membr. Sci. 315 (2008) 28–35, https://doi.org/10.1016/j.memsci.2008.02.002.
[76] P.V. Chai, P.Y. Choy, W.C. Teoh, E. Mahmoudi, W.L. Ang, Graphene oxide based mixed matrix membrane in the presence of eco-friendly natural additive gum Arabic, J. Environ. Chem. Eng. 9 (2021) 105638, https://doi.org/10.1016/j.jece.2021.105638.
[77] X. Sui, Z. Yuan, Y. Yu, K. Goh, Y. Chen, 2D material based advanced membranes for separations in organic solvents, Small 16 (2020) 2003400, https://doi.org/10.1002/smll.202003400.
[78] A. Abdel-Karim, S. Leaper, M. Alberto, A. Vijayaraghavan, X. Fan, S.M. Holmes, E. R. Souaya, M.I. Badawy, P. Gorgojo, High flux and fouling resistant flat sheet polyethersulfone membranes incorporated with graphene oxide for ultrafiltration applications, Chem. Eng. J. 334 (2018) 789–799, https://doi.org/10.1016/j.cej.2017.10.069.
[79] H. Tian, S. Yang, X. Wu, K. Zhang, Two-dimensional molybdenum disulfide oxide (O-MoS2) enhanced tight ultrafiltration membrane with improved molecular separation performance and antifouling properties, Colloids Surfaces A Physicochem. Eng. Asp. 656 (2023) 130328, https://doi.org/10.1016/j.colsurfa.2022.130328.
[80] M. Mirzaei, T. Mohammadi, N. Kasiri, M.A. Tofighy, Fabrication of magnetic field induced mixed matrix membranes containing GO/Fe_3O_4nanohybrids with enhanced antifouling properties for wastewater treatment applications, J. Environ. Chem. Eng. 9 (2021) 105675, https://doi.org/10.1016/j.jece.2021.105675.
[81] G. Zhang, M. Zhou, Z. Xu, C. Jiang, C. Shen, Q. Meng, Guanidyl-functionalized graphene/polysulfone mixed matrix ultrafiltration membrane with superior permselective, antifouling and antibacterial properties for water treatment, J. Colloid Interface Sci. 540 (2019) 295–305, https://doi.org/10.1016/j.jcis.2019.01.050.
[82] S. Arefi-Oskoui, A. Khataee, S. Jabbarvand Behrouz, V. Vatanpour, S. Haddadi Gharamaleki, Y. Orooji, M. Safarpour, Development of MoS_2/O-MWCNTs/PES blended membrane for efficient removal of dyes, antibiotic, and protein, Sep. Purif. Technol. 280 (2022) 119822, https://doi.org/10.1016/j.seppur.2021.119822.
[83] H. Feng, J. Liu, Y. Mu, N. Lu, S. Zhang, M. Zhang, J. Luan, G. Wang, Hybrid ultrafiltration membranes based on PES and MOFs @ carbon quantum dots for improving anti-fouling performance, Sep. Purif. Technol. 266 (2021) 118586, https://doi.org/10.1016/j.seppur.2021.118586.
[84] T. Bohlool, Z. Mohamadnia, Efficient removal of dyes by light-responsive graphene oxide-blended, Polym. Adv. Technol. 34 (2023) 3603–3616, https://doi.org/10.1002/pat.6153.
[85] H. Karimipour, A. Shahbazi, V. Vatanpour, Fouling decline and retention increase of polyethersulfone membrane by incorporating melamine-based dendrimer amine functionalized graphene oxide nanosheets (GO/MDA), J. Environ. Chem. Eng. 9 (2021) 104849, https://doi.org/10.1016/j.jece.2020.104849.
[86] V. Vatanpour, H. Karimi, S. Imanian Ghazanlou, Y. Mansourpanah, M.R. Ganjali, A. Badiei, E. Pourbashir, M.R. Saeb, Anti-fouling polyethersulfone nanofiltration membranes aided by amine-functionalized boron nitride nanosheets with improved separation performance, J. Environ. Chem. Eng. 8 (2020) 104454, https://doi.org/10.1016/j.jece.2020.104454.
[87] D. Lere Keshebo, C.C. Hu, S.T. Kassa, W.S. Hung, C. Feng Wang, S.H. Huang, K. R. Lee, J. Yih Lai, Solvent-exfoliated 2D WS2/Polyethersulfone antifouling mixed matrix ultrafiltration membrane for water treatment, ACS Appl. Polym. Mater. 2 (2020) 5039–5047, https://doi.org/10.1021/acsapm.0c00871.
[88] P. Kallem, N. Elashwah, G. Bharath, H.M. Hegab, S.W. Hasan, F. Banat, Zwitterion-grafted 2D MXene (Ti3C2TX) nanocomposite membranes with improved water permeability and self-cleaning properties, ACS Appl. Nano Mater. 6 (2023) 607–621, https://doi.org/10.1021/acsanm.2c04722.
[89] M.A. Tofighy, T. Mohammadi, Functional charcoal based nanomaterial with excellent colloidal property for fabrication of polyethersulfone ultrafiltration membrane with improved flux and fouling resistance, Mater. Chem. Phys. 285 (2022) 126167, https://doi.org/10.1016/j.matchemphys.2022.126167.